PLOS | PATHOGENS

RESEARCH ARTICLE

T3SS effector VopL inhibits the host ROS response, promoting the intracellular survival of *Vibrio parahaemolyticus*

Marcela de Souza Santos[1], Dor Salomon[1¤], Kim Orth[1,2]*

1 Department of Molecular Biology, University of Texas Southwestern Medical Center, Dallas, Texas, United States of America, **2** Howard Hughes Medical Institute, University of Texas Southwestern Medical Center, Dallas, Texas, United States of America

¤ Current address: Department of Clinical Microbiology and Immunology, Sackler Faculty of Medicine, Tel Aviv University, Tel Aviv, Israel.
* Kim.Orth@utsouthwestern.edu

Citation: de Souza Santos M, Salomon D, Orth K (2017) T3SS effector VopL inhibits the host ROS response, promoting the intracellular survival of *Vibrio parahaemolyticus*. PLoS Pathog 13(6): e1006438. https://doi.org/10.1371/journal.ppat.1006438

Editor: Karla J.F. Satchell, Northwestern University, Feinberg School of Medicine, UNITED STATES

Received: February 8, 2017

Accepted: May 29, 2017

Published: June 22, 2017

Data Availability Statement: All relevant data are within the paper and its Supporting Information files.

Funding: This work was funded by the National Institutes of Health (NIH) grant R01-AI056404, the Welch Foundation grant I-1561, and Once Upon a Time. . .Foundation. MdSS was supported by NIH grant 5T32DK007745-17. The funders had no role in study design, data collection and analysis, decision to publish, or preparation of the manuscript.

Abstract

The production of antimicrobial reactive oxygen species by the nicotinamide dinucleotide phosphate (NADPH) oxidase complex is an important mechanism for control of invading pathogens. Herein, we show that the gastrointestinal pathogen *Vibrio parahaemolyticus* counteracts reactive oxygen species (ROS) production using the Type III Secretion System 2 (T3SS2) effector VopL. In the absence of VopL, intracellular *V. parahaemolyticus* undergoes ROS-dependent filamentation, with concurrent limited growth. During infection, VopL assembles actin into non-functional filaments resulting in a dysfunctional actin cytoskeleton that can no longer mediate the assembly of the NADPH oxidase at the cell membrane, thereby limiting ROS production. This is the first example of how a T3SS2 effector contributes to the intracellular survival of *V. parahaemolyticus*, supporting the establishment of a protective intracellular replicative niche.

Author summary

The marine bacterium *Vibrio parahaemolyticus* is the world's leading cause of food poisoning associated with the consumption of contaminated raw seafood. We recently discovered that during infection, *V. parahaemolyticus* invades cells from the host and uses a suite of effector proteins to convert the invaded cell into a niche for robust bacterial replication. In the present study, we describe how one of the effector proteins, VopL, contributes to this process by disrupting the actin cytoskeleton. Host cells produce reactive oxygen species (ROS) that cause damage to the pathogen's DNA. This ROS production is dependent on a functional actin cytoskeleton. We observed that upon exposure to ROS, the mutant VopL-deficient *V. parahaemolyticus* underwent stress and as a result could not divide, exhibiting a filamentous morphology and concurrent replication impairment. This phenotype can be induced by exposure of the pathogen to ROS. In the presence of VopL, we observed an arrested assembly at the plasma membrane of nicotinamide dinucleotide phosphate (NADPH) oxidase complex, the enzymatic complex that catalyzes the

Competing interests: The authors have declared that no competing interests exist.

generation of ROS. Paralysis of the actin cytoskeleton by VopL results in an inhibition of ROS production, thereby maintaining a relatively stress-free environment within the host cell for *V*. *parahaemolyticus* survival and replication.

Introduction

Vibrio parahaemolyticus is a Gram-negative bacterium that inhabits warm marine and estuarine environments throughout the world [1]. This bacterium is recognized as the world's leading cause of acute gastroenteritis associated with the consumption of contaminated raw or undercooked seafood [2]. In immunocompetent individuals, the illness is self-limiting with symptoms including diarrhea with abdominal cramping, nausea, vomiting, and low-grade fever [1]. However, for individuals with underlying health conditions, the bacterium can breach the gut barrier and cause septicemia corresponding to high mortality rates [3]. *V*. *parahaemolyticus* has also been reported to cause infection of seawater-exposed wounds, which in rare cases escalates to necrotizing fasciitis and septicemia [4]. The bacterium was also identified as the etiologic agent of acute hepatopancreatic necrosis disease (AHPND), a shrimp illness that has recently emerged, causing a massive economic burden on the shrimp industry [5].

Among several virulence factors, including thermostable hemolysins (TDH/TRH), polar and lateral flagella, and adhesins, *V*. *parahaemolyticus* encodes two Type III Secretion Systems (T3SS1 and T3SS2) [6]. These are needle-like apparatuses used by the bacterium to inject proteins, termed effectors, into the host cell [7]. The first T3SS, T3SS1, is present in all sequenced *V*. *parahaemolyticus* strains, including both environmental and clinical isolates, and is induced by culturing the bacteria in low Ca^{2+}, as in serum-free Dulbecco's modified Eagle's medium (DMEM) tissue culture growth medium [8]. While this system does not contribute to the bacterium's enterotoxicity [9], the T3SS1 effectors orchestrate a multifaceted and efficient death of the infected host cell [10]. *V*. *parahaemolyticus* more recently acquired the second T3SS, T3SS2, through a lateral gene transfer event and this system is primarily associated with clinical isolates [6]. The T3SS2 becomes activated in the presence of bile salts [11, 12] and is recognized as the principal virulence factor causing gastroenteritis [9].

We recently reported that during infection, T3SS2 promotes *V*. *parahaemolyticus* invasion of non-phagocytic cells [13, 14]. We found that *V*. *parahaemolyticus* encodes VopC (VPA1321), a deamidase that constitutively activates the GTPases Rac and Cdc42 resulting in membrane ruffling and uptake of the bacterium into the cell [14, 15]. Once inside the host cell, the bacterium is initially contained within an endosome-like vacuole [13]. Upon acidification of the vacuole, but prior to endosome fusion with the lysosome, *V*. *parahaemolyticus* breaks out of its vacuole and escapes into the cytosol [13]. *V*. *parahaemolyticus* then uses the cell as a protected replicative niche (100–300 bacteria/cell) [13]. Although historically studied as an exclusive extracellular bacterium, these findings changed this long-standing view and established *V*. *parahaemolyticus* as a facultative intracellular bacterium. While the role of VopC to promote host cell invasion is well-defined [14], the contribution of other T3SS2 effectors to the maintenance of the intracellular lifecycle of *V*. *parahaemolyticus* remains poorly understood.

VopL (VPA1370), a T3SS2 effector, encodes three consecutive WASP-homology 2 (WH2) domains intermixed with three proline-rich regions and a subsequent VopL C-terminal domain (VCD) (Fig 1A) [16–18]. WH2 domains are commonly found in nucleators of actin filaments; indeed, VopL's *in vitro* nucleating activity is even more potent than that of the maximally-activated Arp2/3 complex [16]. Ectopic expression of VopL in epithelial cells causes a dramatic rearrangement of the actin cytoskeleton into filaments reminiscent of stress fibers

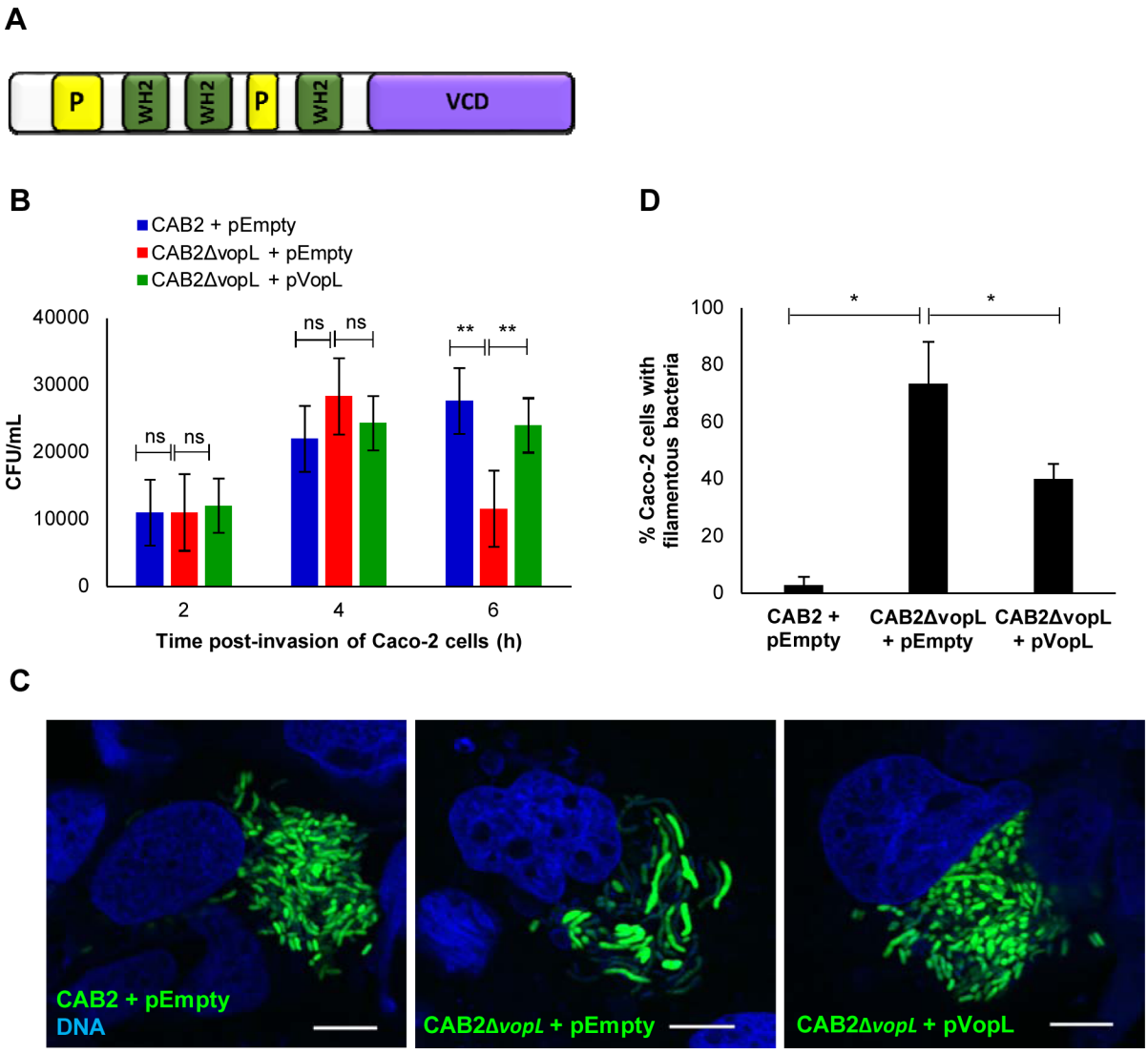

Fig 1. Intracellular CAB2 undergoes filamentation with concurrent decreased survival in the absence of VopL. (A) Schematic of VopL domains: WASP-homology 2 domains (WH2), proline-rich regions (P), and VopL C-terminal domain (VCD). **(B)** Intracellular growth of CAB2 strains in Caco-2 cells. Caco-2 cells were infected with indicated CAB2 strains for 2h followed by incubation with 100 μg/mL gentamicin for the specified times. Cell lysates were serially diluted and plated and CFU was enumerated for intracellular bacteria. Values are means ± SD of a representative experiment performed in triplicate. Asterisks indicate statistically significant difference in intracellular bacteria CFU counts between CAB2 + pEmpty and CAB2Δ*vopL* + pEmpty or between CAB2Δ*vopL* + pEmpty and CAB2Δ*vopL* + pVopL. ** $p < 0.005$. **(C)** Confocal micrographs of Caco-2 cells infected with indicated GFP-tagged CAB2 strains for 2h and incubated with 100 μg/mL gentamicin for 6h. DNA was stained with Hoechst (blue). Scale bars, 10 μm. **(D)** Caco-2 cells invaded by CAB2 + pEmpty, CAB2Δ*vopL* + pEmpty, or CAB2Δ*vopL* + pVopL were enumerated for containment of filamentous bacteria. 90 cells per sample (each sample referring to infection by one of the 3 bacterial strains) were enumerated over 3 independent experiments. Values are means ± SD. Asterisks indicate statistically significant difference between CAB2- and CAB2Δ*vopL*-infection samples (* $p = 0.0116$) or between CAB2Δ*vopL*- and CAB2Δ*vopL* + pVopL-infection samples (* $p = 0.0421$).

https://doi.org/10.1371/journal.ppat.1006438.g001

[16]. Whether VopL nucleates actin from the barbed or pointed end remains a matter of disagreement [19, 20]. Importantly, there is consensus that VopL promotes the nucleation of non-functional filaments in host cells, as opposed *bona fide* to filaments that can be recycled. As a result, VopL arrests actin monomers and the shortage of actin compromises the endogenous assembly of actin networks [19, 20]. Despite the comprehensive characterization of VopL from

a structural and a mechanistic standpoint over the last decade [16, 21], the contribution of this effector during a *V*. *parahaemolyticus* infection remained elusive.

Herein, we show that VopL is required for the intracellular survival of *V*. *parahaemolyticus*. In the absence of VopL, intracellular bacteria filament, which indicates that the bacteria are under stress. We identified the stressor as an increase in exposure to reactive-oxygen species (ROS). We found that the presence of VopL prevented filamentation by suppressing the generation of ROS by the nicotinamide adenine dinucleotide phosphate (NADPH) oxidase complex. To generate ROS, cytosolic and membranous subunits of the NADPH oxidase complex must come together at cell membranes [22]. VopL, by hijacking the actin cytoskeleton, impedes the translocation of NADPH cytosolic subunits to the cell membrane, thereby preventing the complete assembly of the enzymatic ROS complex. Thus, *V*. *parahaemolyticus* deploys the T3SS2 effector VopL to secure a safe replicative niche within the host cell.

Results

In the absence of VopL, *V*. *parahaemolyticus* undergoes filamentation with concurrent decreased intracellular survival

As discussed earlier, despite not contributing to *V*. *parahaemolyticus*' enterotoxicity [9], the T3SS1 becomes activated upon bacterial suspension in DMEM, causing the rapid death (~3h post-infection) of tissue-cultured cells [10], thereby masking the activity of the T3SS2. To reveal the activity of T3SS2 we made use of the *V*. *parahaemolyticus* CAB2 strain, an isogenic strain derived from the clinical isolate RimD2210633 [14]. CAB2 contains a deletion for genes encoding two types of toxic factors. First, a deletion was made in *exsA* loci, resulting in the inactivation of the transcriptional activator for the T3SS1 [23]. Second, deletions were made for *tdhAS*, the two thermostable direct hemolysins (TDH) present in RimD2210633, eliminating their cytotoxic activity [24]. The resulting strain, CAB2, has been used in subsequent studies to assess the activity of T3SS2 and its effectors.

Initially, we set out to investigate the contribution of VopL for the survival of CAB2 within Caco-2 cells, a colonic epithelial cell line. Bacterial survival can be assessed in two ways: first by determining the number of intracellular bacteria as a function of time post-invasion (Fig 1B) and second by visualization of intracellular CAB2 using confocal microscopy (Fig 1C and S1 Fig). Shortly after the invasion of Caco-2 cells (2h post-invasion), CAB2 and its VopL-mutant counterpart (CAB2Δ*vopL*) exhibited comparable cell invasion and intracellular growth (Fig 1B), displaying a patchy distribution inside their host cell (S1A Fig). This activity was reminiscent of *V*. *parahaemolyticus*' vacuolar localization early after invasion [13]. At 4h post-invasion, CAB2 and CAB2Δ*vopL* counts doubled (Fig 1B), consistent with intracellular replication, which was indicated by a significant increase in bacterial load within Caco-2 cells (S1B Fig). At 6h post-invasion, CAB2 exhibited an additional growth increase, while CAB2Δ*vopL* survival was substantially compromised as bacterial counts dropped more than twofold (Fig 1B). Strikingly, confocal inspection of intracellular CAB2Δ*vopL* at 6h post-invasion revealed a dramatic change in bacterial morphology: CAB2 displayed characteristic *V*. *parahaemolyticus*' rod-shape, while CAB2Δ*vopL* appeared significantly elongated (Fig 1C). Expression of VopL in CAB2Δ*vopL* from a plasmid (CAB2Δ*vopL*+pVopL) increased intracellular growth to levels comparable to that of wild type bacteria (Fig 1B) and also rescued normal bacterial morphology (Fig 1C and 1D).

Elongation of CAB2Δ*vopL* was not a result of the cell body extension, but rather a deficiency in bacterial cell division. Closer inspection of CAB2Δ*vopL* revealed that the elongated cell body contained multiple nucleoids (S1C Fig), which is consistent with continuous bacterial replication but ceased septation. This morphological phenotype is referred to as bacterial filamentation and represents an important strategy used by bacteria to survive during stressful

situations [25]. Several bacteria have been reported to undergo filamentation as a protective mechanism against phagocytosis, as in the case of Uropathogenic *Escherichia coli* [26], or against consumption of "inedible" filamentous bacteria by protists, as in the case of *Flectobacillus* spp. [27]. Filamentation can also be triggered in response to DNA-damaging stresses such as UV radiation, antibiotics, and reactive oxygen species (ROS) [25]. Given that CAB2Δ*vopL* deliberately invades Caco-2 cells (via VopC), samples are not exposed to UV radiation, and intracellular bacteria are not exposed to gentamicin, as this antibiotic is not taken up by Caco-2 cells, we hypothesized that host generation of ROS could be responsible for the filamentous CAB2Δ*vopL*.

Bacterial filamentation is ROS-dependent

To investigate whether ROS was causal for filamentation of intracellular CAB2Δ*vopL*, we assessed the generation of ROS inside Caco-2 cells by the nitroblue tetrazolium (NBT) assay [28, 29]. In the NBT assay, the water-soluble tetrazolium dye is reduced by superoxide into blue insoluble formazan deposits, which are readily detectable by microscopic imaging [28, 29]. Uninfected Caco-2 cells displayed little to no formazan precipitates (S2 Fig). Importantly, the accumulation of formazan was substantially greater in cells infected with CAB2Δ*vopL* than in cells infected with wild type CAB2 (S2 Fig), suggesting that VopL plays a role in suppressing the generation of ROS inside the host cell. The accumulation of formazan was observed in Caco-2 cells that contained intracellular bacteria as well as in cells that did not contain bacteria (S2 Fig). These findings support that the presence of extracellular bacteria is sufficient to trigger the host ROS response (possibly via pathogen-associated molecular patterns (PAMPs) such as lipopolysaccharides and flagella). While only a fraction of the host cells were invaded, all cells should be infected, and therefore, receive VopL via T3SS2. Once delivered to infected cells, VopL turns off the ROS response.

Next, we set out to investigate whether bacterial filamentation resulted from ROS production. While formazan deposits could be observed in the minority of Caco-2 cells invaded by rod-shaped, CAB2 bacteria (Fig 2A and 2B), this precipitate was present in about 90% of the cells containing filamentous, CAB2Δ*vopL* bacteria (Fig 2A and 2B). The tight correlation between filamentous bacteria and enriched deposits of formazan strongly implicates ROS as the stressor responsible for CAB2Δ*vopL* filamentation.

ROS can be produced by NADPH oxidases, specialized enzymes whose sole function is the generation of ROS [22]. There are seven members of the NADPH oxidase (NOX) family, NOX1–5 and two dual oxidases (DUOX1 and DUOX2), which collectively produce ROS in a wide range of tissues where ROS participate in a variety of cell processes such as mitogenesis, apoptosis, hormone synthesis, and oxygen sensing [22, 30]. NOX2 is a phagocyte-specific isoform, being highly expressed in neutrophils and macrophages where it plays an essential role in host defense against microbial pathogens [22]. NOX1 is the closest homolog of NOX2, with whom it shares 56% sequence identity [22]. NOX1 is most abundant in the colon epithelium and is also expressed in a variety of cell lines, including Caco-2 cells [30, 31]. At present, the physiological roles of colonic NOX1 are not fully understood. NOX1-derived ROS has been implicated in control of cell proliferation, mucosal repair after injury, and inflammatory response [30]. Importantly, evidence suggests a role for NOX1 as a host defense oxidase [32]. For instance, colon epithelial cells exhibited high NOX1-mediated ROS production in response to flagellin from *Salmonella enteriditis* [33].

In order to assess whether NOX1-dependent generation of ROS played a role for CAB2Δ*vopL* filamentation, we suppressed ROS generation using GKT136901 (GKT), a direct and specific inhibitor of NOX1/4 (NOX4 is primarily expressed in the kidney [22]) [34]. GKT significantly attenuated the accumulation of formazan in Caco-2 cells infected with CAB2Δ*vopL* (S3

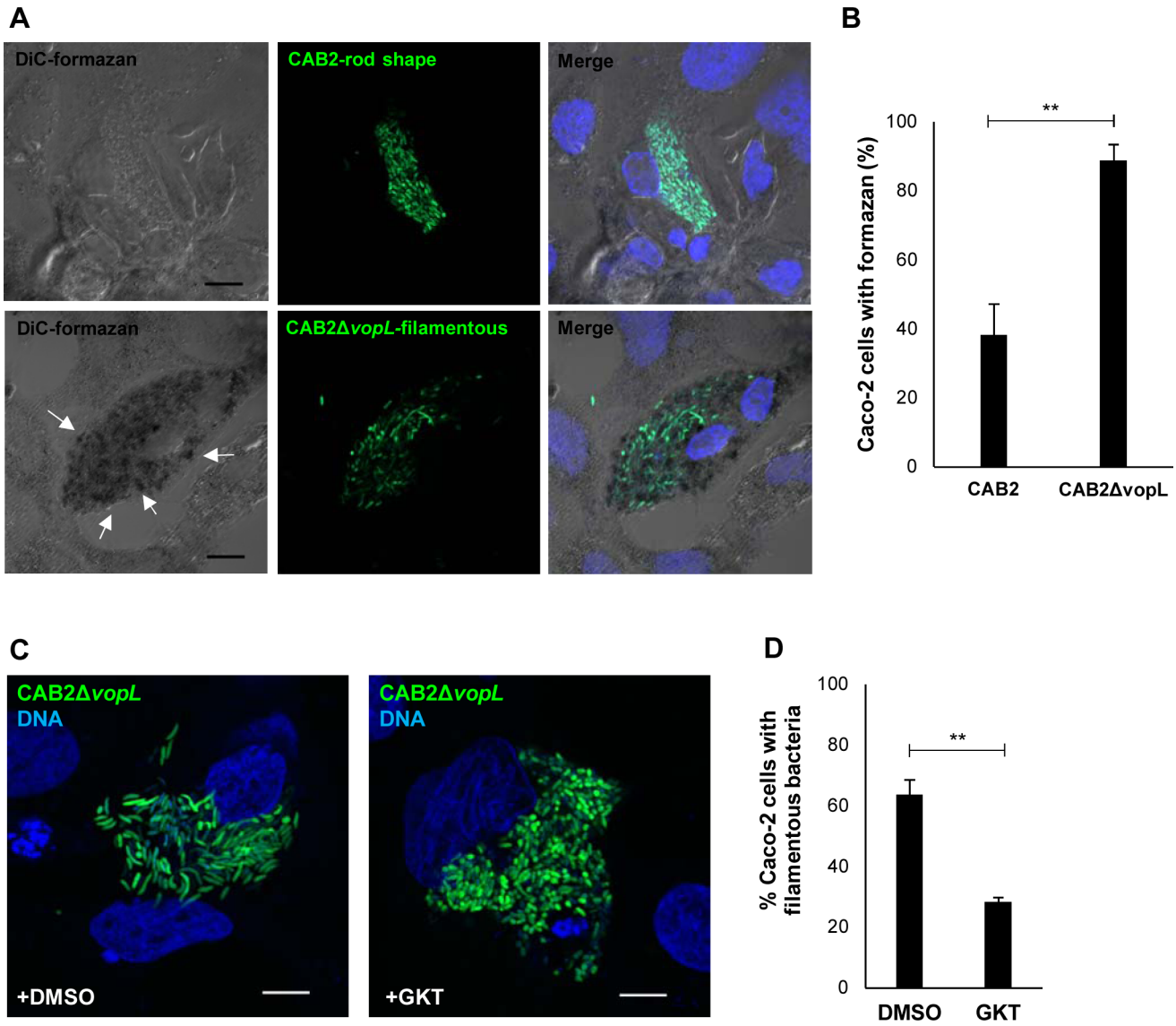

Fig 2. CAB2Δ*vopL* filamentation is ROS-dependent. (A) Confocal micrographs of Caco-2 cells infected with CAB2 (green) or CAB2Δ*vopL*-GFP (green) for 2h followed by incubation with 100 μg/mL gentamicin for 3h. Samples were then incubated with 1 mg/mL NBT for additional 3h in the presence of gentamicin. DNA was stained with Hoechst (blue). Formazan precipitates were visualized in bright field (DiC). White arrows indicate formazan precipitates. Scale bars, 10 μm. (**B**) Quantification of cells containing rod-shaped (CAB2) or filamentous bacteria (CAB2Δ*vopL*) and positive for presence of formazan precipitates. 150 cells for each sample (CAB2 or CAB2Δ*vopL* infections) were analyzed over 3 independent experiments. Values are means ± SD. Asterisks indicate statistically significant difference between CAB2 and CAB2Δ*vopL* samples (** $p = 0.0033$). (**C**) Confocal micrographs of Caco-2 cells infected with CAB2Δ*vopL*-GFP (green) for 2h followed by incubation with 100 μg/mL gentamicin for 6h. Host cells were pre-treated with either dimethyl sulfoxide (DMSO) or 10 μM GKT136901 (GKT), which were kept throughout infection. DNA was stained with Hoechst (blue). Scale bars, 10 μm. (**D**) Quantification of filamentous bacteria in the presence or absence of GKT. Caco-2 cells invaded by CAB2Δ*vopL*-GFP and treated with either DMSO or GKT were analyzed for presence of filamentous bacteria. 300 cells for each sample (DMSO or GKT), over 3 independent experiments, were analyzed for presence of filamentous bacteria. Values are means ± SD. Asterisks indicate statistically significant difference between DMSO and GKT samples (** $p = 0.0038$).

https://doi.org/10.1371/journal.ppat.1006438.g002

Fig), confirming its suitability as an inhibitor of the ROS response. Importantly, this inhibitor reduced the number of host cells containing filamentous CAB2Δ*vopL* by more than twofold (Fig 2C and 2D). As expected, GKT did not affected the intracellular growth of CAB2, given that this strain exhibits minimal filamentation (S4 Fig, Fig 1D). These findings strongly suggest that NOX1-generated ROS mediates bacterial filamentation.

VopL is required for normal bacterial growth in COS^{phox} cells

Our results thus far show that NOX1-generated ROS is causal for bacterial filamentation and that filamentation only occurs in the absence of VopL. Therefore, we hypothesized that VopL suppresses generation of ROS. To quantify NADPH oxidase-dependent production of ROS, we analyzed host cell release of superoxide, the product of NADPH oxidase-mediated reduction of molecular oxygen and the precursor of other ROS [35]. Detection of ROS generated by endogenous NOX1 in the colon, as well as in Caco-2 cells, is challenging to measure [33]. Indeed, under our experimental conditions we could not quantify superoxide in a sensitive manner during infection of Caco-2 cells, nor could we detect it upon cell stimulation with the PKC activator phorbol 12-myristate 13-acetate (PMA) (S5 Fig).

Thus, to further investigate the ability of VopL to control the generation of ROS by NADPH oxidases, we used a well characterized model cell system, the COS^{phox} cell line, that has been used previously to biochemically analyze the production of ROS [36]. These cells stably express NOX2 (gp91^{phox}) along with the other NOX2 complex subunits p22^{phox}, p47^{phox}, and p67^{phox} [36]. Notably, the NOX1 enzymatic complex also includes p22^{phox}, along with NOXO1 and NOXA1, homologs of p47^{phox} and p67^{phox}, respectively [31, 37]. Given the similarity in functioning of the NOX1 and NOX2 complexes, COS^{phox} cells represent a suitable model of non-phagocytic cells with robust NOX-dependent production of ROS for the present study.

Initially, we investigated CAB2 growth within COS^{phox} cells, in the presence and absence of VopL. While CAB2 was able to efficiently replicate inside COS^{phox} cells (Fig 3A) and displayed the bacterium's normal rod-shape (Fig 3B and S6 Fig), CAB2Δ*vopL* grew at approximately half the rate of wild type bacteria (Fig 3A) and, importantly, demonstrated a very dramatic filamentous phenotype (Fig 3B and S6 Fig). Expression of VopL in CAB2Δ*vopL* from a plasmid (CAB2Δ*vopL*+pVopL) rescued intracellular growth to levels comparable to that of wild type bacteria (Fig 3A) and restored the rod-shaped bacterial morphology (Fig 3B and 3C). These findings are in agreement with the observations made using Caco-2 cells and support a role for VopL in bacterial intracellular survival.

Filamentation of Δ*vopL V. parahaemolyticus* within COS^{phox} cells is ROS-dependent

As with Caco-2 cells, we investigated whether filamentation of intracellular CAB2Δ*vopL* resulted from ROS generation by COS^{phox} cells. First, we compared superoxide-mediated accumulation of formazan deposits in COS^{phox} cells containing rod-shaped (CAB2) and filamentous (CAB2Δ*vopL*) bacteria. Formazan precipitates were greatly enriched in host cells containing filamentous bacteria (Fig 4A), being present in about 75% of these cells, a fourfold increase in comparison to cells containing rod-shaped bacteria (Fig 4B). Next, we assessed whether ROS generated in a NOX2-dependent manner was required for bacterial filamentation in COS^{phox} cells. NOX2-dependent generation of ROS was inhibited by apocynin (APO), which blocks ROS generation by preventing the complete assembly of the NOX2 enzymatic complex [22]. APO treatment of COS^{phox} cells abrogated infection-elicited generation of superoxide (S7 Fig) and significantly attenuated CAB2Δ*vopL* filamentation (Fig 4C), reducing the number of COS^{phox} cells containing filamentous bacteria by 40% (Fig 4D). Therefore, in agreement with our findings obtained with Caco-2 cell infection, ROS is an agent involved bacterial filamentation.

VopL suppresses generation of NOX2-derived superoxide

Our results thus far show that VopL impairs the generation of ROS inside Caco-2 and COS^{phox} cells (given as a function of formazan accumulation in these cells). We next set out to quantify

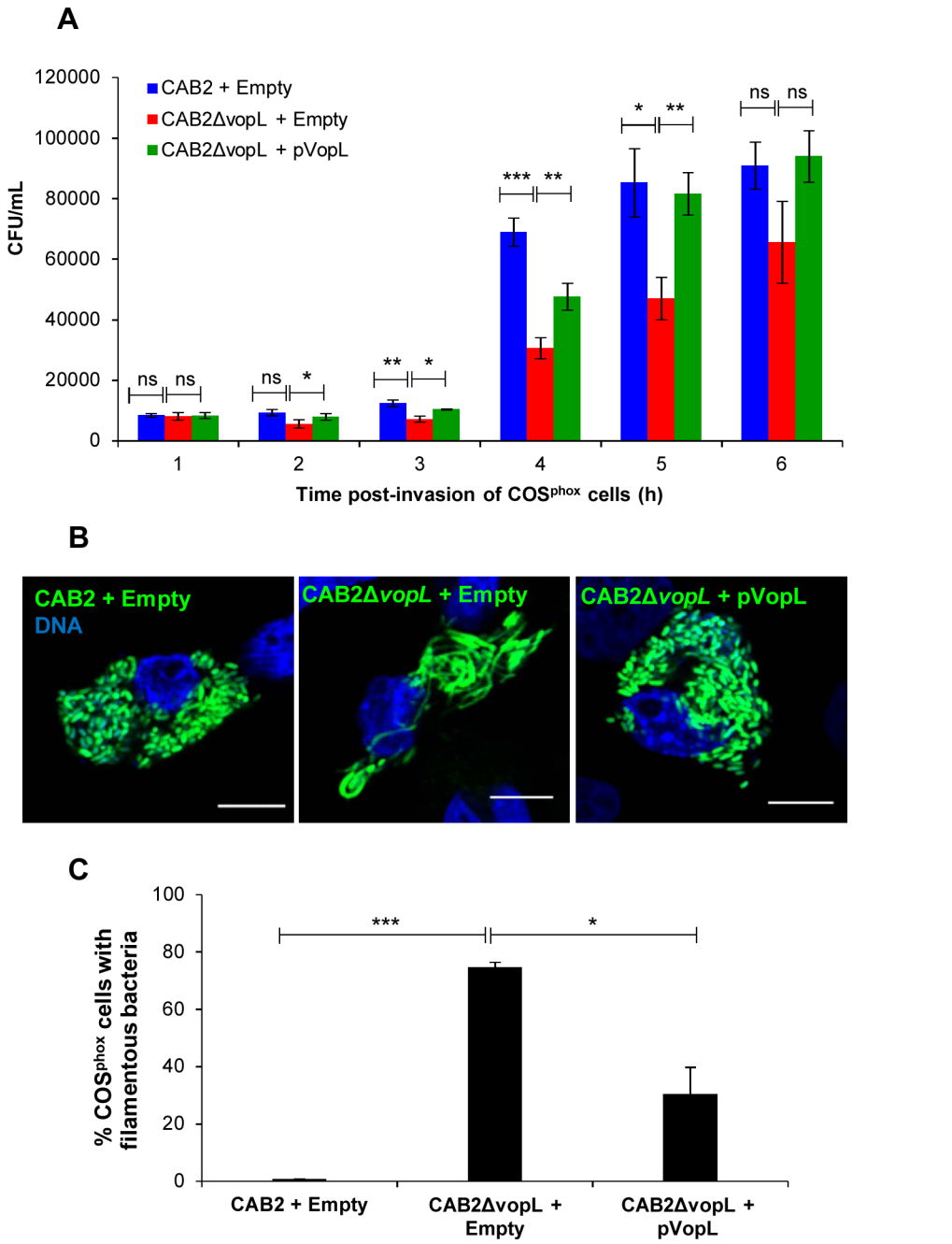

Fig 3. VopL is required for CAB2 survival within COS^{phox} cells. (A) Intracellular growth of CAB2 strains in COS^{phox} cells. COS^{phox} cells were infected with indicated CAB2 strains for 2h followed by incubation with 100 μg/mL gentamicin for the specified times. Cell lysates were serially diluted and plated and CFU was enumerated for intracellular bacteria. Values are means ± SD of a representative experiment performed in triplicate. Asterisks indicate statistically significant difference in intracellular bacteria CFU counts between CAB2 + pEmpty and CAB2Δ*vopL* + pEmpty or between CAB2Δ*vopL* + pEmpty and CAB2Δ*vopL* + pVopL. * $p < 0.05$, ** $p < 0.005$, *** $p < 0.0005$. **(B)** Confocal micrographs of COS^{phox} cells infected with indicated GFP-tagged CAB2 strains for 2h and incubated with 100 μg/mL gentamicin for 6h. DNA was stained with Hoechst (blue). Scale bars, 10 μm. **(C)** COS^{phox} cells invaded by CAB2 + pEmpty, CAB2Δ*vopL* + pEmpty, or CAB2Δ*vopL* + pVopL were enumerated for containment of filamentous bacteria. 90 cells per sample (each sample referring to infection by one of the 3 bacterial strains) were enumerated over 3 independent experiments. Values are means ± SD. Asterisks indicate statistically significant difference between CAB2- and CAB2Δ*vopL*-infection samples (*** $p = 0.0002$) or between CAB2Δ*vopL*- and CAB2Δ*vopL* + pVopL-infection samples (* $p = 0.0122$).

https://doi.org/10.1371/journal.ppat.1006438.g003

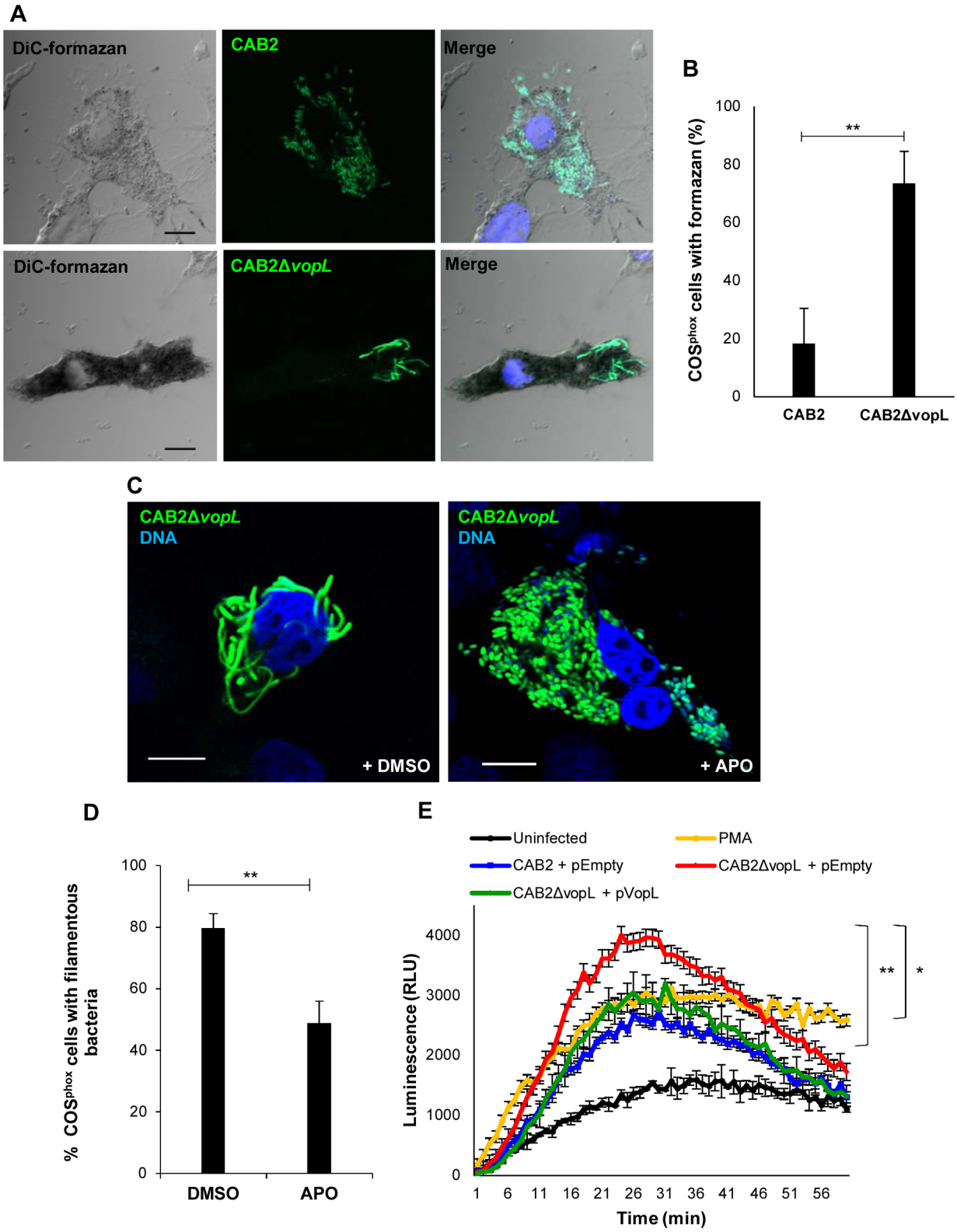

Fig 4. VopL inhibits generation of superoxide. (A) Confocal micrographs of COS^{phox} cells infected with CAB2 (green) or CAB2Δ*vopL*-GFP (green) for 2h followed by incubation with 100 μg/mL gentamicin for 4h. Samples were then incubated with 1 mg/mL NBT for additional 1h in the presence of gentamicin. DNA was stained with Hoechst (blue). Formazan precipitates were visualized in bright field (DiC). Scale bars, 10 μm. (**B**) Quantification of cells containing rod-shaped (CAB2) or filamentous bacteria (CAB2Δ*vopL*)

and positive for presence of formazan precipitates. 150 cells for each sample (CAB2 or CAB2Δ*vopL* infections) were analyzed over 3 independent experiments. Values are means ± SD. Asterisks indicate statistically significant difference between CAB2 and CAB2Δ*vopL* samples (** $p = 0.0031$). (**C**) Confocal micrographs of COS^{phox} cells infected with CAB2Δ*vopL*-GFP (green) for 2h followed by incubation with 100 μg/mL gentamicin for 6h. At the beginning of the last hour of gentamicin incubation, either dimethyl sulfoxide (DMSO) or 250 μM APO was added to the samples. DNA was stained with Hoechst (blue). Scale bars, 10 μm. **(D)** Quantification of filamentous bacteria in the presence or absence of APO. COS^{phox} cells invaded by CAB2Δ*vopL*-GFP and treated with either DMSO or APO were analyzed for presence of filamentous bacteria. 300 cells for each sample (DMSO or APO), over 3 independent experiments, were analyzed for presence of filamentous bacteria. Values are means ± SD. Asterisks indicate statistically significant difference between DMSO and APO samples (** $p = 0.0058$). **(E)** COS^{phox} cells were infected with indicated CAB2 strains for 2h after which cells were incubated with luminol substrate and luminescence was measured over 1h. Values are means ± SD from one representative experiment. Asterisks indicate statistically significant difference between CAB2- and CAB2Δ*vopL*-infection samples (** $p = 0.0039$) or between CAB2Δ*vopL*- and CAB2Δ*vopL* + pVopL-infection samples (* $p = 0.0387$) at minute 26 (peak of luminescence signal).

https://doi.org/10.1371/journal.ppat.1006438.g004

the production of ROS in the absence and presence of VopL. To quantify the production of ROS, we measured the extracellular release of superoxide by COS^{phox} cells as a function of luminescence [35].

As a control for NOX2-dependent generation of superoxide, we stimulated COS^{phox} cells with PMA. PMA activates the NOX2 complex via PKC-mediated phosphorylation of the p47^{phox} subunit [38]. Cell stimulation with PMA led to a sustained generation of superoxide (Fig 4E). Infection of COS^{phox} cells with CAB2 induced the production of superoxide, which peaked at around 26 min post luminol addition and tapered off afterwards due to lack of continuous bacterial stimulus (bacteria washed away prior to luminol addition) (Fig 4E). Importantly, bacteria-stimulated generation of ROS is substantially enhanced in the absence of VopL, as the peak in luminescence signal (at 26 min) during CAB2Δ*vopL* infection is 1.7 times higher than the luminescence peak resulting from CAB2 infection (Fig 4E). Rescue of the CAB2Δ*vopL* strain with a VopL-expression plasmid lowered superoxide production to levels similar to that generated by the parental CAB2 strain (Fig 4E). These results confirm our hypothesis that VopL suppresses NOX-generated ROS.

VopL suppresses the movement of NOX cytosolic subunits to cell membranes

As mentioned earlier, NOX2 is a multi-subunit complex; the latent complex is disassembled in resting cells and must become assembled at cell membranes with potential to generate ROS [22]. When at rest, the NOX2 complex regulatory subunits p67^{phox} and p47^{phox} are present in the cytosol as a heterotrimeric complex along with p40^{phox} [22]. Rac, another complex subunit, is also present in the cytosol in its inactive, GDP-bound, form. Upon cell stimulation, all activated cytosolic components translocate to both cell plasma and phagocytic membranes where they interact with membranous subunits gp91^{phox} (NOX2) and p22^{phox} and complete the assembly of a functional NOX complex [22]. Several pieces of evidence support a role for actin in NOX2 activity. For instance, addition of G-actin was shown to potentiate NOX activity in a cell-free system [39]. The p47^{phox} and p67^{phox} each contain a SH3 domain known to associate with the actin cytoskeleton [38]. In resting polymorphonuclear leukocytes (PMN), p67^{phox} is detected exclusively in the detergent-insoluble, cytoskeletal fraction [38]. Additionally, inhibition of actin polymerization by cytochalasin has been shown to modulate the translocation of NOX2 subunits from the cytosol to the plasma membrane upon stimulation of PMNs [40, 41].

Despite the close homology between the NOX1 and NOX2 complexes (the closest homologs within the NOX family), NOXO1, the homolog of p47^{phox} in the NOX1 complex, lacks the autoinhibitory region (AIR) domain present in p47^{phox} [31, 37]. As a result, NOXO1, as well as its partner NOXA1 (p67^{phox} homolog), are constitutively associated with p22^{phox} at the cell membrane [42]. Importantly, Rac1 is not constitutively localized to cell membranes. In

fact, stimulated recruitment of Rac1 from the cytosol to cell membranes is crucial to the activation of NOXA1, and thereby, the NOX1 complex [43]. Additionally, Rac1 promotes further recruitment of NOXA1 to cell membranes [43].

Given that VopL disrupts the normal assembly of the actin cytoskeleton, we hypothesized that this effector inhibited an actin-dependent step that is common to the activation of both NOX1 and NOX2 complexes. This step was hypothesized to be the recruitment of cytosolic subunits of NOX1 (Rac1) and NOX2 ($p47^{phox}$, $p67^{phox}$, Rac1) to cell membranes. Initially we investigated the NOX2 complex activation expressed in COS^{phox} cells. To test our hypothesis, we transiently transfected COS^{phox} cells with VopL and subsequently induced NOX2 activation using PMA. Cell stimulation with PMA caused $p67^{phox}$ to translocate from the cytosol to the plasma membrane and also caused an extensive rearrangement of the actin cytoskeleton with formation of membrane ruffles that co-localized with $p67^{phox}$ (compare S8A and S8B Fig). As previously reported [16], ectopic expression of wild type VopL (WT VopL) caused the formation of long actin strings reminiscent of stress fibers (Fig 5A and S8C Fig). In cells transfected with WT VopL, PMA-stimulated actin ruffles were not formed (Fig 5A) and, importantly, the translocation of $p67^{phox}$ from the cytosol to the cell membrane was impaired (Fig 5A). Quantification of enrichment of $p67^{phox}$ at the plasma membrane revealed a significantly smaller presence of this subunit at the membrane in the presence of VopL (Fig 5B).

To confirm that the inhibitory effect of VopL on $p67^{phox}$ translocation is dependent on the effector's ability to manipulate the actin cytoskeleton, we also transfected cells with WH2*3-VopL, which contains point mutations at amino acids required for the actin binding activity of the WH2 domains [16]. We previously established that WH2*3-VopL is devoid of actin assembly activity *in vitro* and does not induce actin stress fiber formation in transfected cells [16] (S8D Fig). Expression of WH2*3-VopL impaired neither PMA-stimulated membrane ruffling nor the cytosol-plasma membrane translocation of $p67^{phox}$ (Fig 5C), which was highly enriched at the plasma membrane (Fig 5D).

During activation of the NOX2 complex, the stimulated recruitment of Rac to the membrane occurs independently from $p47^{phox}$ or $p67^{phox}$ [44]. Therefore, we also investigated whether VopL-mediated disruption of the actin cytoskeleton impaired translocation of Rac. To monitor Rac movement, COS^{phox} cells were transiently transfected with EGFP-Rac1 with either WT or WH2*3-VopL. As was observed with $p67^{phox}$, cells stimulated with PMA caused Rac1 to translocate from the cytosol to the plasma membrane (compare S9A and S9B Fig). At the plasma membrane, Rac1 co-localized with actin ruffles (S9B Fig). Importantly, expression of WT VopL completely inhibited PMA-stimulation recruitment of Rac1 to the plasma membrane (S9C and S9E Fig), while in cells expressing WH2*3-VopL, the cytosol-plasma membrane translocation of Rac1 was unaffected (S9D and S9E Fig).

Next, we set out to determine if VopL could also inhibit stimulated recruitment of Rac1 to the plasma membrane in Caco-2 cells. Upon cell stimulation with PMA, Rac1 moved to the plasma membrane and co-localized with the actin ruffles (compare Fig 6A and 6B). When cells were co-transfected with Rac1 and wild-type VopL, but not mutant WH2*3-VopL, Rac1 remained in the cytosol (Fig 6C–6E). Therefore, VopL deploys a general mechanism to cripple the defenses of the host cell: it paralyzes the actin cytoskeleton, preventing assembly of both NOX1 and NOX2 complex, thereby inhibiting the generation of ROS during infection.

Jasplakinolide phenocopies VopL-mediated inhibition of NOX2 complex assembly

VopL rearranges the actin cytoskeleton into linear strings of non-functional filaments that resemble stress fibers (Fig 5A). By doing so, VopL retains $p67^{phox}$ and Rac1 in the cytosol, and

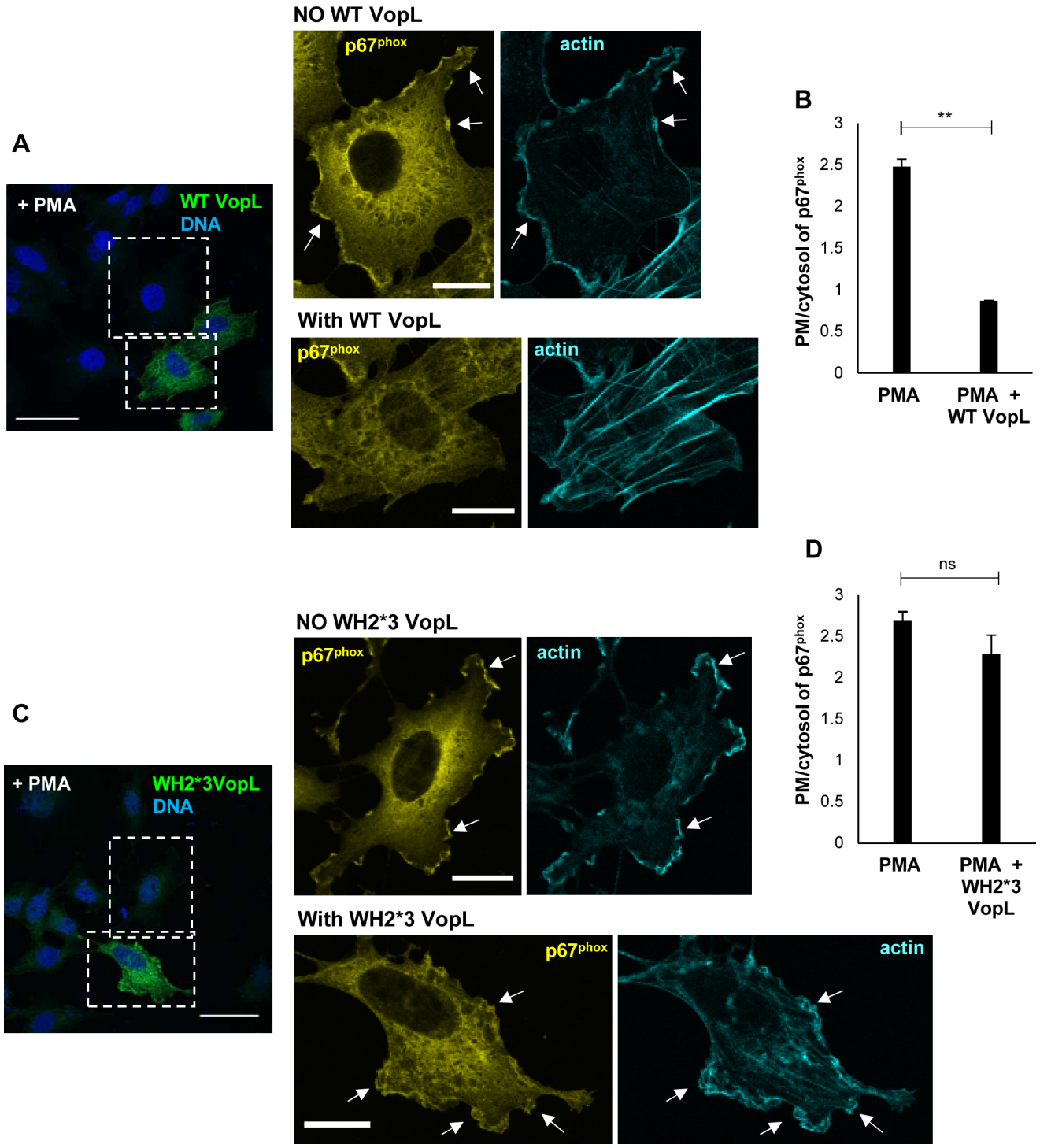

Fig 5. VopL inhibits assembly of NOX2 complex. COS^{phox} cells were transiently transfected with either wild type VopL (WT VopL, panel **A**) or catalytically inactive VopL (WH2*3-VopL, panel **C**) and subsequently stimulated for ROS response with 0.4 μg/mL phorbol 12-myristate 13-acetate (PMA). Cells were immunostained for p67^{phox} (pseudo-colored in yellow to enhance contrast) and VopL (green). DNA and actin were stained with Hoechst (blue) and Alexa Fluor 680 phalloidin (pseudo-colored in cyan to enhance contrast), respectively. White, dotted boxes highlight regions within untransfected and transfected cells that were magnified. Scale bars, 40 μm (larger panels) and 10 μm (individuals cells). **(B,D)** PMA-stimulated translocation of p67^{phox} from the cytosol to the plasma membrane, for untransfected cells and cells transfected with either WT VopL **(B)** or WH2*3-VopL **(D)**, was quantified by analysis of line scans crossing the two cellular compartments. 90 cells for each population (untransfected or transfected with VopL) were analyzed over 3 independent experiments. Values are means ± SD. Asterisk indicates statistically significant difference between untransfected and WT VopL-transfected cells (** $p = 0.0011$).

https://doi.org/10.1371/journal.ppat.1006438.g005

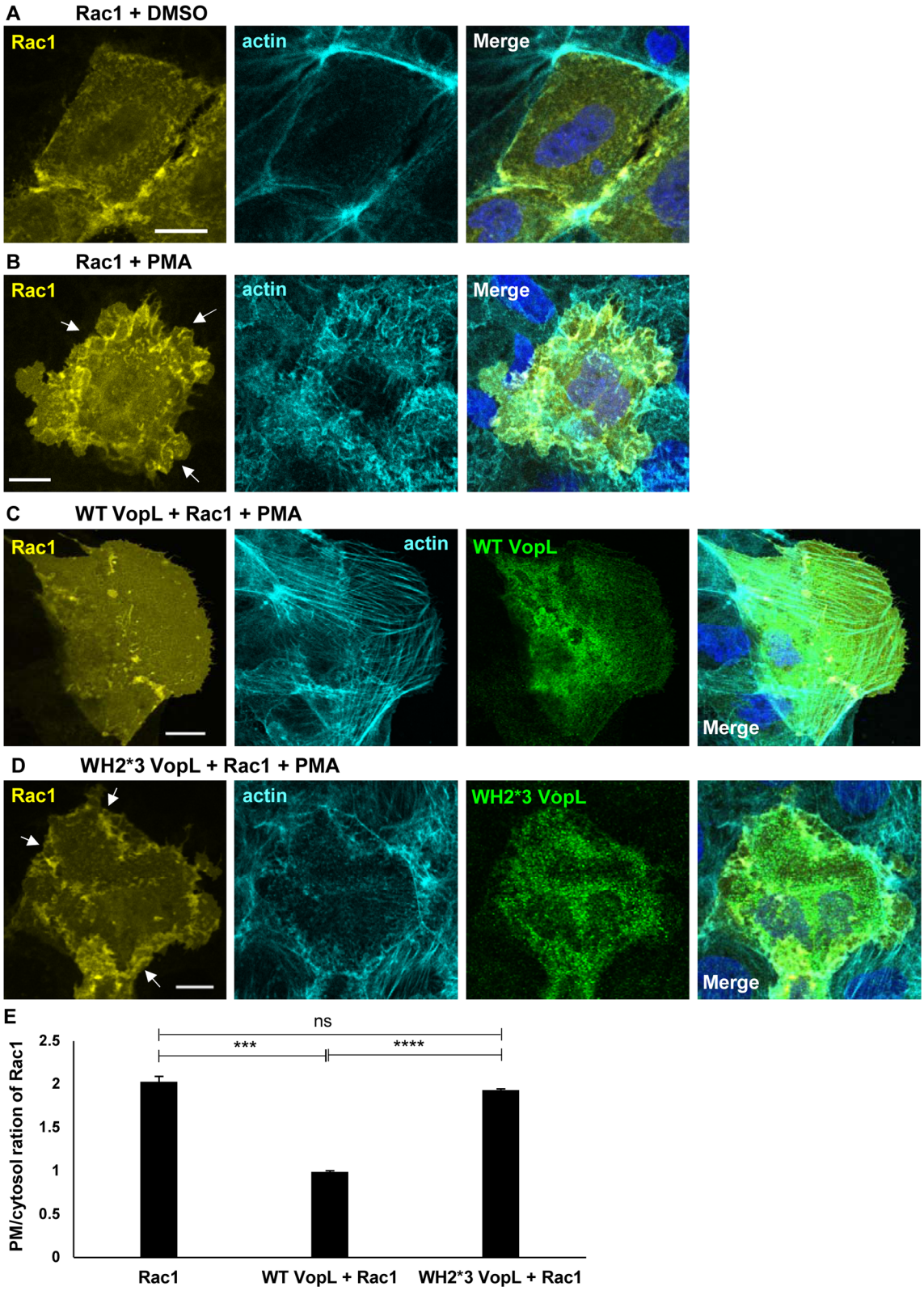

Fig 6. VopL inhibits Rac1 recruitment to NOX1 complex. Caco-2 cells were transiently transfected with EGFP-Rac1 and treated only with vehicle (DMSO, **A**) or stimulated with 1 μg/mL phorbol 12-myristate 13-acetate (PMA, **B**). Additionally, PMA-stimulated cells were transiently transfected with either wild type VopL (WT VopL, panel **C**) or catalytically inactive

VopL (WH2*3-VopL, panel **D**). Cells were immunostained for VopL (pseudo-colored in green to enhance contrast). EGFP-Rac1 was pseudo-colored in yellow to enhance contrast. DNA and actin were stained with Hoechst (blue) and Alexa Fluor 680 phalloidin (pseudo-colored in cyan to enhance contrast), respectively. White arrows indicate membrane ruffles. Scale bars, 15 μm. **(E)** PMA-stimulated translocation of Rac1 from the cytosol to the plasma membrane, for cells transfected with either WT VopL or WH2*3-VopL, was quantified by analysis of line scans crossing the two cellular compartments. 75 cells for each population (Rac1 only or Rac1 + VopL WT/WH2*3) were analyzed over 3 independent experiments. Values are means ± SD. Asterisk indicates statistically significant difference between Rac1 and Rac1 + VopL WT transfected cells (** $p = 0.0006$) as well as between Rac1 and Rac1 + VopL WH2*3 transfected cells (*** $p = 0.0001$).

https://doi.org/10.1371/journal.ppat.1006438.g006

consequently, impedes the activation of NOX2. Therefore, we assessed whether manipulation of the actin cytoskeleton in the form of stable stress fiber-like structures could account for the inhibition of NOX2 assembly.

Jasplakinolide is a potent inducer of actin polymerization and a stabilizer of actin filaments [45]. Treatment of COS^{phox} cells with jasplakinolide induced stress fiber formation (compare Fig 7A and 7B). As with VopL, jasplakinolide treatment decreased PMA-stimulated translocation of $p67^{phox}$ from the cytosol to the plasma membrane (compare Fig 7C and 7D). However, in contrast to VopL transfected cells treated with PMA, actin ruffles are observed at the edges of cells treated with jasplakinolide and PMA (Figs 5A and 7D, respectively). These findings further support our hypothesis that VopL manipulates the actin cytoskeleton to prevent NOX assembly and dampen ROS production.

Discussion

The T3SS2 effector VopL and its *V*. *cholerae* homologue VopF were discovered about a decade ago and their structure and biochemical activities are now well-characterized [16–19, 46–48]. The coincidental discoveries that VopL/F produces non-functional filaments [19, 20] and our findings that *V*. *parahaemolyticus* is a facultative intracellular pathogen [13] laid the groundwork for the elucidation of the biological role of VopL during infection. Here, we showed that NOX-derived generation of ROS plays an important role in controlling intracellular proliferation of *V*. *parahaemolyticus*. Specifically, ROS-dependent stress of the bacterium resulted in impairment of cell division and consequent filamentation of the bacteria. VopL is essential in preventing this deleterious event: by directly targeting the actin cytoskeleton and catalyzing the assembly of non-canonical actin filaments, VopL arrests the actin-dependent movement of cytosolic NOX subunits to cell membranes. As a result, VopL prevents the activation of the NOX complex and consequent production of ROS. Thus, this is the first report of how VopL aids *V*. *parahaemolyticus* infection: it secures a relatively "stress-free" environment within the host cell, enabling the bacterium to establish a successful replicative niche.

Previous studies indicated that VopL does not play a significant role in bacterial colonization and fluid accumulation in the small intestine of rabbit models of *V*. *parahaemolyticus* infection [49, 50]. Our present findings support that VopL could have an understated contribution to enterotoxicity, not obvious in the pathogenesis markers evaluated so far, prompting future investigations of a role for VopL in a diarrheogenic model.

Distinct methods are used by other intracellular pathogens to inhibit ROS-mediated killing. Some pathogens scavenge ROS using extracellular polysaccharides, as in the case of *Burkholderia cenocepacia* and *Pseudomonas aeruginosa* [51, 52]. Several other pathogens act on signaling machinery upstream of ROS and prevent activation of the NOX complex. [53–56]. *Salmonella enterica* Typhimurium excludes the NOX2 membranous subunits from the vacuole it inhabits in a T3SS-dependent manner [57]. Importantly, the virulence factors and mechanisms used by the vast majority of these pathogens remain unknown. The present work not only identified the

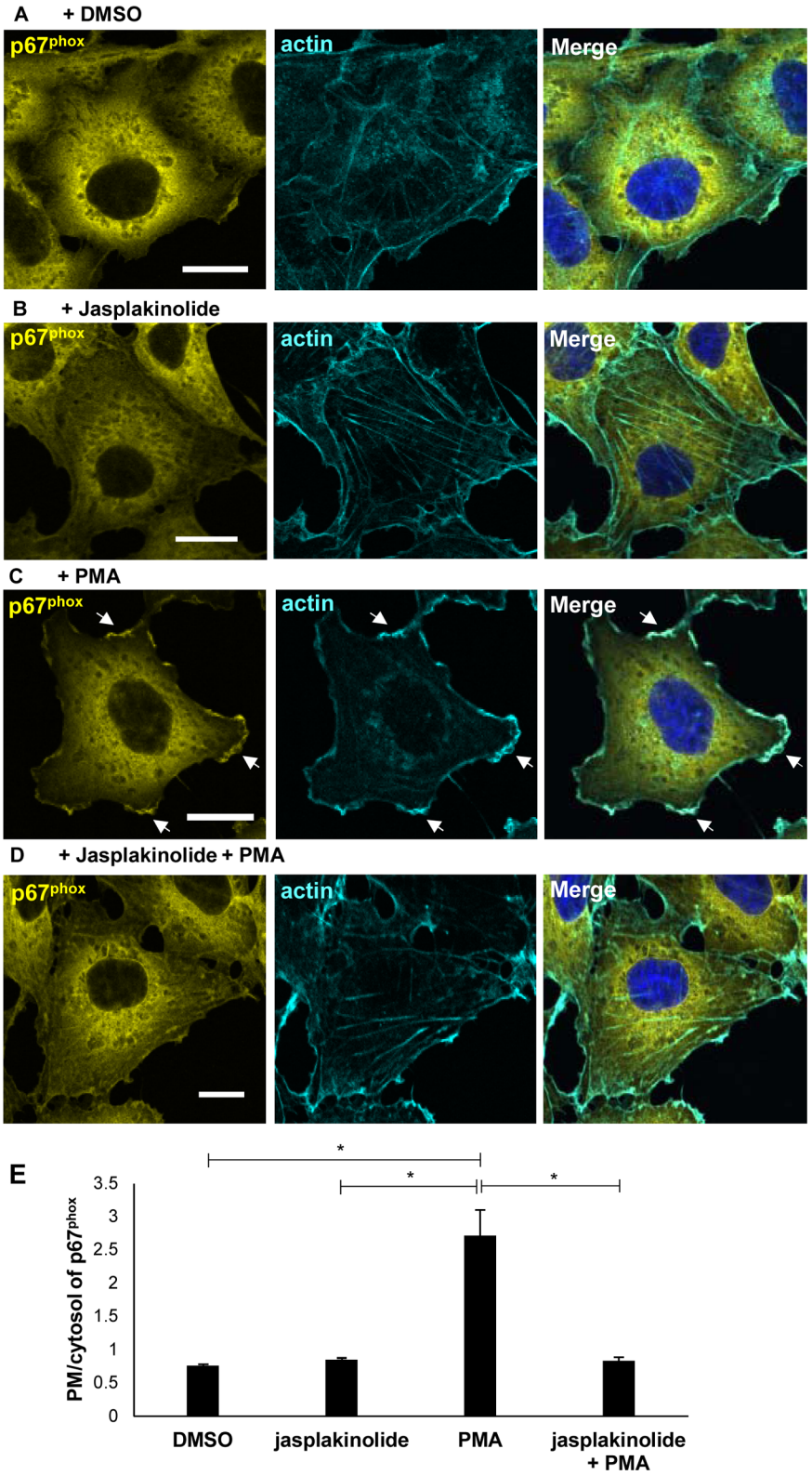

Fig 7. Jasplakinolide arrests assembly of NOX2 complex. COS^{phox} cells were treated with either DMSO **(A)** or 100 nM jasplakinolide **(B)** and subsequently stimulated for ROS response with 0.4 μg/mL phorbol 12-myristate 13-acetate (PMA) **(C,D)**. Cells were immunostained for p67^{phox} (pseudo-colored in yellow to enhance contrast). DNA and actin were stained with Hoechst (blue) and Alexa Fluor 680 phalloidin (pseudo-

colored in cyan to enhance contrast), respectively. Scale bars, 20 μm. **(E)** PMA-stimulated translocation of $p67^{phox}$ from the cytosol to the plasma membrane, for cells transfected with jasplakinolide or left untreated, was quantified by analysis of line scans crossing the two cellular compartments. 90 cells for each population (DMSO treatment only, jasplakinolide-treated only, PMA-stimulated, or jasplakinolide+PMA treated) were analyzed over 3 independent experiments. Values are means ± SD. Asterisk indicates statistically significant difference between mock (DMSO) or PMA stimulated cells (* $p = 0.0126$), between jasplakinolide or PMA-treated cells (* $p = 0.0136$), and between PMA-stimulated or jasplakinolide+PMA treated cells (* $p = 0.0127$).

https://doi.org/10.1371/journal.ppat.1006438.g007

virulence factor used by *V*. *parahaemolyticus* to suppress host ROS generation, but also revealed an unprecedented mechanism used by a microbial pathogen to do so (Fig 8).

The pharmacological inhibition of NOX1 and NOX2 complexes, shown to fully suppress ROS generation in the case of apocynin, did not result in complete reduction of bacterial filamentation. These findings raise the possibility that additional factors may contribute to the arrest of bacterial division. Intracellular growth of certain *Salmonella* strains resulted in filamentous bacteria due to a defect in the bacterial histidine biosynthetic pathway [58]. Because *V*. *parahaemolyticus* only undergoes filamentation in the absence of VopL, under our experimental conditions, it is likely that host factors, rather than bacterial ones, elicit this morphological phenotype. Rosenberger and Finlay [59] reported an upregulation of MEK1 kinase during *S*. *enterica* Typhimurium infection of RAW 264.7 macrophages. MEK upregulation was causal for *Salmonella* filamentation, as occurrence of filamentous bacteria partially decreased in the presence of MEK inhibitors [59]. MEK and NOX activities operated in parallel to mediate *Salmonella* filamentation [59]. It is known that the actin cytoskeleton functions as a scaffold that mechanically modulates the activation of signaling pathways [60]. For instance, pharmacological inhibition of the actin polymerization reportedly inhibited ERK and AKT activation [61]. Interestingly, *V*. *parahaemolyticus* expresses VopA, a homolog of *Yersinia* spp. YopJ Ser/Thr acetyltransferase that has been shown to inhibit MAPK signaling pathways during infection [62–64]. Therefore, in addition to NOX assembly and MAPK signaling pathways, other pathways will be the subject of future investigation as further mediators of filamentation of the VopL-mutant.

As discussed earlier, the T3SS2 is *V*. *parahaemolyticus*' key virulence mechanism of enterotoxicity [9]. Importantly, T3SS2 is orthologous to the T3SS identified in several non-O1, non-O129 clinical *V*. *cholerae* strains [65]. These strains lack cholera toxin and toxin-coregulated pilus but cause acute diarrheal diseases in a T3SS-dependent manner [46]. The non-O1, non-O129 AM-19226 strain encodes VopL's homolog VopF (32% sequence identity and 72% sequence similarity) [46]. VopF induces actin-rich protrusion formation as opposed to actin stress fibers [46]. By disrupting the actin cytoskeleton, VopF causes depolarization of the epithelium and *vopF*-mutant strains present deficient epithelial colonization *in vivo* [47]. Therefore, despite the fact that VopL and VopF share close structural homology and use the same strategy to disrupt the actin cytoskeleton, these two effectors equip their bacteria with two distinct pathogenic mechanisms. Notably, the non-O1, non-O139 strain 1587 encodes VopN, which shares similarity with both VopF and VopL [47]. VopN also nucleates actin filaments, and, like VopL, localizes to actin stress fibers [47]. While the physiological role of VopN remains elusive, we recently reported that the VopN-encoding strain 1587 invades epithelial cells in a T3SS-dependent manner [14].

Over many years of evolution, *V*. *parahaemolyticus*' T3SS2 has maintained a repertoire of around a dozen effectors. One of these, VopC, has been shown to mediate cell invasion, and we now show a role for VopL in relieving free-radical stress for this intracellular pathogen. The activities of some of the other T3SS2 effectors have been studied and now the role that they play in this evolutionarily conserved invasive T3SS are ripe for future investigation.

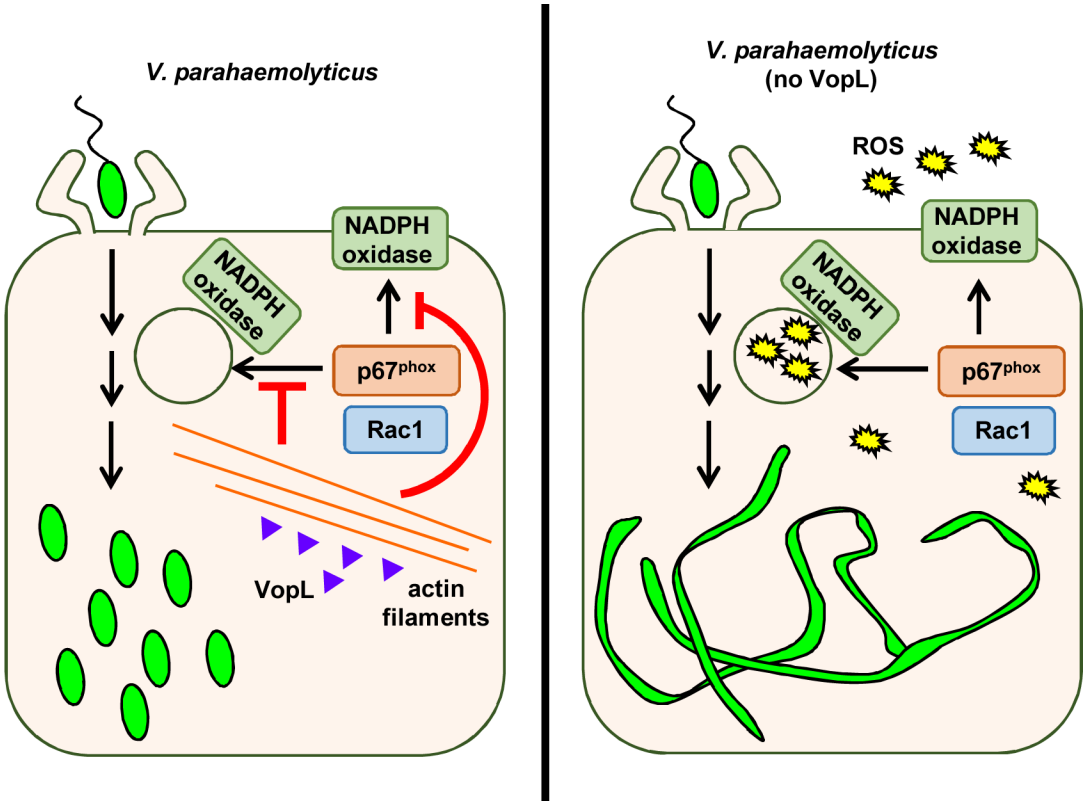

Fig 8. VopL inhibits NOX-derived production of ROS. *V. parahaemolyticus* deploys its T3SS2 effector VopL to disrupt the actin cytoskeleton. As a result, NOX cytosolic regulatory subunits do not translocate to cell membranes. In the absence of VopL, NOX-mediated generation of ROS induces bacterial stress, leading to bacterial filamentation.

https://doi.org/10.1371/journal.ppat.1006438.g008

Materials and methods

Bacterial strains and culture conditions

The *V. parahaemolyticus* CAB2 strain was derived from POR1 (clinical isolate RIMD2210633 lacking TDH toxins), the latter being a generous gift from Drs. Tetsuya Iida and Takeshi Honda [66]. The CAB2 strain was made by deleting the gene encoding the transcriptional factor ExsA, which regulates the activation of the T3SS1 [14]. CAB2 was grown in Luria-Bertani (LB) medium, supplemented with NaCl to a final concentration of 3% (w/v), at 30 ˚C. When necessary, the medium was supplemented with 50 μg/mL spectinomycin (to select for growth of CAB2-GFP strains [9]) or 250 μg/mL kanamycin.

Deletion of *vopL* from CAB2 strain

For in-frame deletion of *vopL* (*vpa1370* in RimD2210633, GeneBank sequence accession number NC_004605), the nucleotide sequences 1kb upstream and downstream of the gene were cloned into pDM4, a Cm^r Ori6RK suicide plasmid [14]. Primers used were 5' GATCGTCG ACATCAAATTGAATGCACTATGATC 3' and 5' GATCACTAGTAAAGAAGACCCCTTT ATTGATTC 3' for amplification of 1kb upstream region, and 5' GATCACTAGTCTAGCG AGCACATAAAAAGC 3' and 5' GATCAGATCTTCCGGGGTGGTAAATGCTT3' for 1kb downstream region. 1kb sequences were then inserted between SalI and SpeI sites (upstream region) or SpeI and BglII (downstream region) sites of the plasmid multiple cloning site. The resulting construct was inserted into CAB2 via conjugation by S17-1 (*λpir*) *Escherichia coli*.

Transconjugants were selected for on minimal marine medium (MMM) agar containing 25 μg/mL chloramphenicol. Subsequent bacterial growth on MMM agar containing 15% (w/v) allowed for counter selection and curing of *sacB*-containing pDM4. Deletion was confirmed by PCR and sequencing analysis.

Reconstitution of CAB2Δ*vopL*

For reconstitution of CAB2Δ*vopL*, the sequence coding for *vopL* + FLAG tag was amplified using primers 5' GATCCTGCAGATGCTTAAAATTAAACTGCCT 3' and 5' GATA GAAT TC TTA CTTATCGTCGTCATCCTTGTAATC CGATAATTTTGCAGATAGTGC 3' and then cloned into the pBAD/*Myc*-His vector (Invitrogen, resistance changed from ampicillin to kanamycin) between PstI and EcoRI sites. The 1kb nucleotide sequence upstream of *vopC* (*vpa1321* in RimD2210633, accession numberNC_004605.1) was used as a promoter and cloned between XhoI and PstI sites using the primers 5' GATC CTCGAG TATTCTTAATA AGTCAGGAGG 3' and 5'GATC CTCGAG TATTCTTAATAAGTCAGGAGG3'. The resulting construct was inserted into CAB2Δ*vopL* via triparental conjugation using *E. coli* DH5α (pRK2073). Transconjugants were selected for on MMM agar containing 250 μg/mL kanamycin. Reconstitution was confirmed by PCR. Empty pBAD plasmid (without *vopL* gene insertion) was introduced to CAB2 and CAB2Δ*vopL* strains for consistency in bacterial strain manipulation.

Mammalian cell culture

Caco-2 cells (ATCC, Manassas, VA) were maintained in Minimal Essential Medium with Earl's Balanced Salts (MEM/EBSS, Hyclone, Logan, UT), supplemented with 20% (v/v) fetal bovine serum (Sigma-Aldrich, St. Louis, MO), 1% (v/v) penicillin-streptomycin (Thermo Fisher Scientific, Waltham, MA), and kept at 5% CO_2 and 37˚C. COS^{phox} cells were grown in low-glucose Dulbecco's Modified Eagle's Medium (DMEM, Thermo Fisher Scientific) supplemented with 10% (v/v) fetal bovine serum, 1% (v/v) penicillin-streptomycin, 1% (v/v) sodium pyruvate (Thermo Fisher Scientific), 0.8 mg/mL G418 (Thermo Fisher Scientific), 200 μg/mL hygromycin (Thermo Fisher Scientific), and 1 μg/mL puromycin (Thermo Fisher Scientific), at 37˚C with 5% CO_2 [35].

Infection of tissue culture cells

Caco-2 and COS^{phox} cells were seeded onto 24-well plates at a density of $2.5x10^5$ (Caco-2) or $1.5x10^5$ cells/well (COS^{phox}) and grown for 18–20 h. Overnight-grown bacterial cultures were normalized to an optical density at 600 nm (OD_{600}) of 0.3 and then grown in MLB supplemented with 0.05% (w/v) bile salts for 90 min at 37˚C. Growth in the presence of bile salts allowed for induction of T3SS2 [11, 12]. Mammalian host cells were subsequently infected with CAB2 strains at a multiplicity of infection (MOI) of 10 using culture medium devoid of antibiotics (infection medium). To synchronize infection, cell plates were centrifuged at 200x *g* for 5 minutes. Infection was carried out for 2 h at 37˚C, after which cells were washed with unsupplemented MEM/EBSS or DMEM and subsequently treated with infection medium containing 100 μg/mL gentamicin for 1–6 h. At the end of each time point, host cells were washed with 1x PBS for removal of extracellular dead bacteria and lysed with 0.5% (v/v) TX-100. Cell lysates were serially diluted and plated on MMM agar for counting of colony forming units (CFU) as a measurement of intracellular bacterial survival/replication. To analyze bacterial filamentation, host cells were counted as containing filamentous bacteria when the cell predominantly contained bacteria longer than wild-type (CAB2) size bacteria. Filamentous

bacteria needed to be at least twice the size the size of wild-type CAB2 to be considered filamentous.

Where indicated, samples were pre-treated with 10 μM GKT136901 (GKT, Aobious, Gloucester, MA) or added with 250 μM apocynin (APO, Sigma-Aldrich) at the remaining last 1 hour of infection or last hour of gentamicin incubation (6^{th} hour).

Microscopic NBT assay

Caco-2/COS^{phox} cells were left uninfected or infected as described above. Within 3 (Caco-2) or 4 (COS^{phox}) hours of gentamicin incubation, cell media was replaced with fresh media containing 1 mg/mL nitroblue tetrazolium (NBT, Sigma-Aldrich) and gentamicin for additional 3 (Caco-2) or 1 (COS^{phox}) hour. GKT or DMSO were added where indicated. Samples were then process for confocal analysis as described below.

Quantification of superoxide production

Caco-2 or COS^{phox} cells were seeded onto 6-well plates at $5x10^5$ cells/well and infected with CAB2 strains for 2 h as described above. Cells were trypsinized (0.25% trypsin/EDTA), centrifuged at 200x *g* for 5 min, and resuspended in Hank's Balanced Salt Solution (HBSS, ThermoFisher) supplemented with Ca^{2+} and Mg^{2+}. Superoxide production was measured as a function of emission of luminescence using the Diogenes kit (National Diagnostics Lab, Atlanta, GA) and according to the manufacturer's protocol [35]. Luminescence was monitored over 60 minutes using a FluoStar Optima plate reader.

Transient transfection of mammalian cells

Caco-2 and COS^{phox} cells were transiently transfected with 0.3 μg of either wild type (WT) VopL-Flag-psFFV or catalytically inactive VopL-WH2x3*-Flag-psFFV constructs [16], 0.5 μg of pcDNA3-EGFP-Rac1 [67] (plasmid # 12980, Addgene, Cambridge, MA) + 1.2 μg of empty psFFV using Fugene HD (Promega) for COS^{phox} cells or Lipofectamine LTX with PLUS reagent (ThermoFisher) for Caco-2 cells for 20–24 h. Subsequently, COS^{phox}/Caco-2 cells were treated with 0.4/1.0 μg/mL phorbol 12-myristate 13-acetate (PMA, Sigma-Aldrich) for 10/30 min at 37˚C.

Confocal microscopy imaging

For imaging, Caco-2 and COS^{phox} cells were seeded respectively at $2.5x10^5$ and $1\text{-}2x10^5$cells/well onto 6-well plates containing UV-sterilized, poly-L-lysine-coated (Sigma), glass coverslips. Following the infection and transfection protocols described above, samples were fixed with 3.2% (v/v) *ρ*-formaldehyde (Thermo Fisher Scientific) for 10 minutes at room temperature. Transfected COS^{phox} cells were permeabilized with 0.5% (w/v) saponin (Sigma) for 10 minutes at room temperature and then blocked with 1% (w/v) bovine serum albumin (BSA, Sigma-Aldrich) in the presence of 0.1% saponin for 30 minutes at room temperature. In order to detect cells transfected with VopL, samples were subsequently incubated with anti-Flag antibody (1:100 dilution in 0.5% BSA, 0.1% saponin [Cell Signaling, #2368, Danvers, MA]) for 1 hour at room temperature, followed by incubation with anti-rabbit Alexa Fluor 488/A555 conjugated secondary antibody (1:500 dilution in 0.5% BSA, 0.1% saponin [Thermo Fisher Scientific, A-21441]) for another 1h, room temperature. For detection of $p67^{phox}$, samples were incubated with anti-$p67^{phox}$ at 1:50 dilution (Santa Cruz, sc-7662, Dallas, TX), followed by incubation with anti-goat Alexa Fluor 555 conjugated secondary antibody (1:500 dilution [Thermo Fisher Scientific, A-21432]).

F-actin was stained with 2 units/mL of either rhodamine- or Alexa Fluor 680-phalloidin (Thermo Fisher Scientific) and DNA was stained with 1 μg/mL Hoechst A33342 (Invitrogen, Carlsbad, CA). Coverslips were placed sample-side down on glass slides containing Prolong Gold anti-fade mounting media (Thermo Fisher Scientific) and imaged on Zeiss LSM710 and LSM800 confocal microscopes. Images were converted using ImageJ (NIH).

Statistical analysis

All data are given as mean ± standard deviation from at least 3 independent experiments unless stated otherwise. Each experiment was conducted in triplicate. Statistical analyses were performed by using unpaired, two-tailed Student's t test with Welch's correction. A p value of < 0.05 was considered significant.

Supporting information

S1 Fig. *V. parahaemolyticus* undergoes filamentation in the absence of VopL. (A,B) Confocal micrographs of Caco-2 cells infected with indicated GFP-tagged CAB2 strains for 2h and incubated with 100 μg/mL gentamicin for **(A)** 2h or **(B)** 4h. DNA was stained with Hoechst (blue). Scale bars, 10 μm. **(C)** Confocal micrograph highlights filamentous bacteria containing multiple nucleoids. Dotted white boxes indicate magnified bacteria. White arrows indicate bacterial nucleoids.
(TIF)

S2 Fig. VopL inhibits ROS response in Caco-2 cells. Confocal micrographs of Caco-2 cells left uninfected or infected with either CAB2-GFP (green) or CAB2Δ*vopL*-GFP (green) for 2h followed by incubation with 100 μg/mL gentamicin for 3h. Samples were then incubated with 1 mg/mL NBT for additional 3h in the presence of gentamicin. DNA was stained with Hoechst (blue). Formazan precipitates were visualized in bright field (DiC). Scale bars, 100 μm.
(TIF)

S3 Fig. GTK suppresses intracellular generation of ROS. Confocal micrographs of Caco-2 cells left uninfected or infected with CAB2Δ*vopL*-GFP (green) for 2h followed by incubation with 100 μg/mL gentamicin for 3h. Samples were then incubated with 1 mg/mL NBT for additional 3h in the presence of gentamicin. Host cells were pre-treated with either dimethyl sulfoxide (DMSO) or 10 μM GKT136901 (GKT), which were kept throughout infection. DNA was stained with Hoechst (blue). Formazan precipitates were visualized in bright field (DiC). Scale bars, 100 μm.
(TIF)

S4 Fig. GKT does not affect intracellular growth of CAB2. (A) Confocal micrographs of Caco-2 cells infected with CAB2-GFP (green) for 2h followed by incubation with 100 μg/mL gentamicin for 6h. Host cells were pre-treated with either dimethyl sulfoxide (DMSO) or 10 μM GKT136901 (GKT), which were kept throughout infection. DNA was stained with Hoechst (blue). Scale bars, 10 μm. (**B**) Quantification of filamentous bacteria in the presence or absence of GKT. Caco-2 cells invaded by CAB2-GFP and treated with either DMSO or GKT were analyzed for presence of filamentous bacteria. 300 cells for each sample (DMSO or GKT), over 3 independent experiments, were analyzed for presence of filamentous bacteria. Values are means ± SD. Difference in number of Caco-2 cells containing filamentous bacteria between DMSO- and GKT-treated samples was not statistically significant.
(TIF)

S5 Fig. Low production of superoxide from Caco-2 cells. Caco-2 and COS^{phox} cells were left untreated or treated with 0.4 μg/mL phorbol 12-myristate 13-acetate (PMA) and superoxide production was measured as a function of luminescence intensity. Values are means ± SD from one representative experiment.
(TIF)

S6 Fig. Filamentous growth of CAB2Δ*vopL* within COS^{phox} cells. Confocal micrographs of Caco-2 cells infected with indicated GFP-tagged CAB2 strains for 2h and incubated with 100 μg/mL gentamicin for 3-5h. DNA was stained with Hoechst (blue). Scale bars, 10 μm.
(TIF)

S7 Fig. Apocynin suppresses bacterial-induced generation of superoxide. COS^{phox} cells were infected with indicated CAB2Δ*vopL* for 2h. 1h prior to the end of the infection, 250 μM apocynin (APO) was added and superoxide production was measured as a function of luminescence intensity. As a positive control of suppression of superoxide, 50 units of superoxide dismutase were added at the end of infection. Values are means ± SD from one representative experiment.
(TIF)

S8 Fig. VopL disrupts the actin cytoskeleton. COS^{phox} cells were stimulated for ROS production with 0.4 μg/mL phorbol 12-myristate 13-acetate (PMA, panel **B**). Cells treated with only vehicle (dimethyl sulfoxide, DMSO) were left unstransfected (**A**) or transiently transfected with either wild type VopL (WT VopL, panel **C**) or catalytically inactive VopL (VopL-WH2x3*, panel **D**). Cells were immunostained for p67^{phox} (pseudo-colored in yellow to enhance contrast) and VopL (green). DNA and actin were stained with Hoechst (blue) and Alexa Fluor 680 phalloidin (pseudo-colored in cyan to enhance contrast), respectively. Scale bars, 40 μm.
(TIF)

S9 Fig. VopL inhibits stimulated recruitment of Rac1 to the plasma membrane. COS^{phox} cells were transiently transfected with EGFP-Rac1 and treated only with vehicle (DMSO, **A**) or stimulated with 0.4 μg/mL phorbol 12-myristate 13-acetate (PMA, **B**). Additionally, PMA-stimulated cells were transiently transfected with either wild type VopL (WT VopL, panel **C**) or catalytically inactive VopL (WH2*3-VopL, panel **D**). Cells were immunostained for VopL (pseudo-colored in green to enhance contrast). EGFP-Rac1 was pseudo-colored in yellow to enhance contrast. DNA and actin were stained with Hoechst (blue) and Alexa Fluor 680 phalloidin (pseudo-colored in cyan to enhance contrast), respectively. Scale bars, 40 μm. **(E)** PMA-stimulated translocation of Rac1 from the cytosol to the plasma membrane in cells transfected only with Rac1 or transfected with both Rac1 and VopL WT/WH2*3 was monitored. Quantification was performed by analysis of line scans crossing the two cellular compartments. 90 cells for each population (Rac1 only or Rac1 + VopL WT/WH2*3) were analyzed over 3 independent experiments. Values are means ± SD. Asterisk indicates statistically significant difference between Rac1 and Rac1 + VopL WT transfected cells (** $p = 0.0074$) as well as between Rac1 and Rac1 + VopL WH2*3 transfected cells (*** $p = 0.0005$).
(TIF)

Acknowledgments

We thank Dr. Mary C. Dinauer for the valuable contribution of the COS^{phox} cell line. We also thank the members of the Orth lab for discussion and technical assistance.

Author Contributions

Conceptualization: MdSS DS KO.

Data curation: MdSS.

Formal analysis: MdSS.

Funding acquisition: MdSS KO.

Investigation: MdSS.

Methodology: MdSS DS KO.

Project administration: MdSS DS KO.

Resources: KO.

Supervision: KO.

Validation: MdSS DS KO.

Visualization: MdSS.

Writing – original draft: MdSS DS KO.

Writing – review & editing: MdSS DS KO.

References

1. Marcela de Souza Santos DS, Peng Li, Krachler Anne-Marie, Kim Orth. Vibrio parahaemolyticus virulence determinants. In: Joseph Alouf DL, Popff Michel R., editor. The Comprehensive Sourcebook of Bacterial Toxins. Fourth ed: Elsevier; 2015. p. 230–60.
2. O'Boyle N, Boyd A. Manipulation of intestinal epithelial cell function by the cell contact-dependent type III secretion systems of Vibrio parahaemolyticus. Front Cell Infect Microbiol. 2014; 3:114. https://doi.org/10.3389/fcimb.2013.00114 PMID: 24455490; PubMed Central PMCID: PMCPMC3887276.
3. Daniels NA, MacKinnon L, Bishop R, Altekruse S, Ray B, Hammond RM, et al. Vibrio parahaemolyticus infections in the United States, 1973–1998. J Infect Dis. 2000; 181(5):1661–6. https://doi.org/10.1086/315459 PMID: 10823766.
4. Tena D, Arias M, Alvarez BT, Mauleon C, Jimenez MP, Bisquert J. Fulminant necrotizing fasciitis due to Vibrio parahaemolyticus. J Med Microbiol. 2010; 59(Pt 2):235–8. https://doi.org/10.1099/jmm.0.014654-0 PMID: 19797463.
5. Lee CT, Chen IT, Yang YT, Ko TP, Huang YT, Huang JY, et al. The opportunistic marine pathogen Vibrio parahaemolyticus becomes virulent by acquiring a plasmid that expresses a deadly toxin. Proc Natl Acad Sci U S A. 2015; 112(34):10798–803. https://doi.org/10.1073/pnas.1503129112 PMID: 26261348; PubMed Central PMCID: PMCPMC4553777.
6. Makino K, Oshima K, Kurokawa K, Yokoyama K, Uda T, Tagomori K, et al. Genome sequence of Vibrio parahaemolyticus: a pathogenic mechanism distinct from that of V cholerae. Lancet. 2003; 361(9359):743–9. https://doi.org/10.1016/S0140-6736(03)12659-1 PMID: 12620739.
7. Galan JE, Wolf-Watz H. Protein delivery into eukaryotic cells by type III secretion machines. Nature. 2006; 444(7119):567–73. https://doi.org/10.1038/nature05272 PMID: 17136086.
8. Ono T, Park KS, Ueta M, Iida T, Honda T. Identification of proteins secreted via Vibrio parahaemolyticus type III secretion system 1. Infect Immun. 2006; 74(2):1032–42. https://doi.org/10.1128/IAI.74.2.1032-1042.2006 PMID: 16428750; PubMed Central PMCID: PMCPMC1360304.
9. Ritchie JM, Rui H, Zhou X, Iida T, Kodoma T, Ito S, et al. Inflammation and disintegration of intestinal villi in an experimental model for Vibrio parahaemolyticus-induced diarrhea. PLoS Pathog. 2012; 8(3):e1002593. https://doi.org/10.1371/journal.ppat.1002593 PMID: 22438811; PubMed Central PMCID: PMCPMC3305451.
10. Burdette DL, Yarbrough ML, Orvedahl A, Gilpin CJ, Orth K. Vibrio parahaemolyticus orchestrates a multifaceted host cell infection by induction of autophagy, cell rounding, and then cell lysis. Proc Natl Acad Sci U S A. 2008; 105(34):12497–502. https://doi.org/10.1073/pnas.0802773105 PMID: 18713860; PubMed Central PMCID: PMCPMC2527940.

11. Gotoh K, Kodama T, Hiyoshi H, Izutsu K, Park KS, Dryselius R, et al. Bile acid-induced virulence gene expression of Vibrio parahaemolyticus reveals a novel therapeutic potential for bile acid sequestrants. PLoS One. 2010; 5(10):e13365. https://doi.org/10.1371/journal.pone.0013365 PMID: 20967223; PubMed Central PMCID: PMCPMC2954181.
12. Li P, Rivera-Cancel G, Kinch LN, Salomon D, Tomchick DR, Grishin NV, et al. Bile salt receptor complex activates a pathogenic type III secretion system. Elife. 2016; 5. https://doi.org/10.7554/eLife.15718 PMID: 27377244; PubMed Central PMCID: PMCPMC4933562.
13. de Souza Santos M, Orth K. Intracellular Vibrio parahaemolyticus escapes the vacuole and establishes a replicative niche in the cytosol of epithelial cells. MBio. 2014; 5(5):e01506–14. https://doi.org/10.1128/mBio.01506-14 PMID: 25205094; PubMed Central PMCID: PMCPMC4173779.
14. Zhang L, Krachler AM, Broberg CA, Li Y, Mirzaei H, Gilpin CJ, et al. Type III effector VopC mediates invasion for Vibrio species. Cell Rep. 2012; 1(5):453–60. https://doi.org/10.1016/j.celrep.2012.04.004 PMID: 22787576; PubMed Central PMCID: PMCPMC3392014.
15. Okada R, Zhou X, Hiyoshi H, Matsuda S, Chen X, Akeda Y, et al. The Vibrio parahaemolyticus effector VopC mediates Cdc42-dependent invasion of cultured cells but is not required for pathogenicity in an animal model of infection. Cell Microbiol. 2014; 16(6):938–47. https://doi.org/10.1111/cmi.12252 PMID: 24345190; PubMed Central PMCID: PMCPMC4670550.
16. Liverman AD, Cheng HC, Trosky JE, Leung DW, Yarbrough ML, Burdette DL, et al. Arp2/3-independent assembly of actin by Vibrio type III effector VopL. Proc Natl Acad Sci U S A. 2007; 104(43):17117–22. https://doi.org/10.1073/pnas.0703196104 PMID: 17942696; PubMed Central PMCID: PMCPMC2040399.
17. Namgoong S, Boczkowska M, Glista MJ, Winkelman JD, Rebowski G, Kovar DR, et al. Mechanism of actin filament nucleation by Vibrio VopL and implications for tandem W domain nucleation. Nat Struct Mol Biol. 2011; 18(9):1060–7. https://doi.org/10.1038/nsmb.2109 PMID: 21873985; PubMed Central PMCID: PMCPMC3173040.
18. Yu B, Cheng HC, Brautigam CA, Tomchick DR, Rosen MK. Mechanism of actin filament nucleation by the bacterial effector VopL. Nat Struct Mol Biol. 2011; 18(9):1068–74. https://doi.org/10.1038/nsmb.2110 PMID: 21873984; PubMed Central PMCID: PMCPMC3168117.
19. Avvaru BS, Pernier J, Carlier MF. Dimeric WH2 repeats of VopF sequester actin monomers into non-nucleating linear string conformations: An X-ray scattering study. J Struct Biol. 2015; 190(2):192–9. https://doi.org/10.1016/j.jsb.2015.03.008 PMID: 25818509.
20. Burke TA, Harker AJ, Dominguez R, Kovar DR. The bacterial virulence factors VopL and VopF nucleate actin from the pointed end. J Cell Biol. 2017. doi: 10.1083/jcb.201608104 PMID: 28363971.
21. Dominguez R. The WH2 Domain and Actin Nucleation: Necessary but Insufficient. Trends Biochem Sci. 2016; 41(6):478–90. https://doi.org/10.1016/j.tibs.2016.03.004 PMID: 27068179; PubMed Central PMCID: PMCPMC4884163.
22. Bedard K, Krause KH. The NOX family of ROS-generating NADPH oxidases: physiology and pathophysiology. Physiol Rev. 2007; 87(1):245–313. https://doi.org/10.1152/physrev.00044.2005 PMID: 17237347.
23. Zhou X, Shah DH, Konkel ME, Call DR. Type III secretion system 1 genes in Vibrio parahaemolyticus are positively regulated by ExsA and negatively regulated by ExsD. Mol Microbiol. 2008; 69(3):747–64. https://doi.org/10.1111/j.1365-2958.2008.06326.x PMID: 18554322; PubMed Central PMCID: PMCPMC2610376.
24. Park KS, Ono T, Rokuda M, Jang MH, Iida T, Honda T. Cytotoxicity and enterotoxicity of the thermostable direct hemolysin-deletion mutants of Vibrio parahaemolyticus. Microbiol Immunol. 2004; 48(4):313–8. PMID: 15107542.
25. Justice SS, Hunstad DA, Cegelski L, Hultgren SJ. Morphological plasticity as a bacterial survival strategy. Nat Rev Microbiol. 2008; 6(2):162–8. https://doi.org/10.1038/nrmicro1820 PMID: 18157153.
26. Justice SS, Hunstad DA, Seed PC, Hultgren SJ. Filamentation by Escherichia coli subverts innate defenses during urinary tract infection. Proc Natl Acad Sci U S A. 2006; 103(52):19884–9. https://doi.org/10.1073/pnas.0606329104 PMID: 17172451; PubMed Central PMCID: PMCPMC1750882.
27. Hahn MW, Moore ER, Hofle MG. Bacterial filament formation, a defense mechanism against flagellate grazing, is growth rate controlled in bacteria of different phyla. Appl Environ Microbiol. 1999; 65(1):25–35. PMID: 9872755; PubMed Central PMCID: PMCPMC90978.
28. Wang T, Malawista SE, Pal U, Grey M, Meek J, Akkoyunlu M, et al. Superoxide anion production during Anaplasma phagocytophila infection. J Infect Dis. 2002; 186(2):274–80. https://doi.org/10.1086/341451 PMID: 12134266.
29. Roos D, de Boer M. Molecular diagnosis of chronic granulomatous disease. Clin Exp Immunol. 2014; 175(2):139–49. https://doi.org/10.1111/cei.12202 24016250; PubMed Central PMCID: PMCPMC3892405. PMID: 24016250

30. Geiszt M, Leto TL. The Nox family of NAD(P)H oxidases: host defense and beyond. J Biol Chem. 2004; 279(50):51715–8. https://doi.org/10.1074/jbc.R400024200 PMID: 15364933.

31. Geiszt M, Lekstrom K, Witta J, Leto TL. Proteins homologous to p47phox and p67phox support superoxide production by NAD(P)H oxidase 1 in colon epithelial cells. J Biol Chem. 2003; 278(22):20006–12. https://doi.org/10.1074/jbc.M301289200 PMID: 12657628.

32. Sirokmany G, Donko A, Geiszt M. Nox/Duox Family of NADPH Oxidases: Lessons from Knockout Mouse Models. Trends Pharmacol Sci. 2016; 37(4):318–27. https://doi.org/10.1016/j.tips.2016.01.006 PMID: 26861575.

33. Kawahara T, Kuwano Y, Teshima-Kondo S, Takeya R, Sumimoto H, Kishi K, et al. Role of nicotinamide adenine dinucleotide phosphate oxidase 1 in oxidative burst response to Toll-like receptor 5 signaling in large intestinal epithelial cells. J Immunol. 2004; 172(5):3051–8. PMID: 14978110.

34. Teixeira G, Szyndralewiez C, Molango S, Carnesecchi S, Heitz F, Wiesel P, et al. Therapeutic potential of NADPH oxidase 1/4 inhibitors. Br J Pharmacol. 2016. https://doi.org/10.1111/bph.13532 PMID: 27273790.

35. Woolery AR, Yu X, LaBaer J, Orth K. AMPylation of Rho GTPases subverts multiple host signaling processes. J Biol Chem. 2014; 289(47):32977–88. https://doi.org/10.1074/jbc.M114.601310 PMID: 25301945; PubMed Central PMCID: PMCPMC4239643.

36. Price MO, McPhail LC, Lambeth JD, Han CH, Knaus UG, Dinauer MC. Creation of a genetic system for analysis of the phagocyte respiratory burst: high-level reconstitution of the NADPH oxidase in a nonhematopoietic system. Blood. 2002; 99(8):2653–61. PMID: 11929750.

37. Takeya R, Ueno N, Kami K, Taura M, Kohjima M, Izaki T, et al. Novel human homologues of p47phox and p67phox participate in activation of superoxide-producing NADPH oxidases. J Biol Chem. 2003; 278(27):25234–46. https://doi.org/10.1074/jbc.M212856200 PMID: 12716910.

38. Nauseef WM, Volpp BD, McCormick S, Leidal KG, Clark RA. Assembly of the neutrophil respiratory burst oxidase. Protein kinase C promotes cytoskeletal and membrane association of cytosolic oxidase components. J Biol Chem. 1991; 266(9):5911–7. PMID: 1848559.

39. Morimatsu T, Kawagoshi A, Yoshida K, Tamura M. Actin enhances the activation of human neutrophil NADPH oxidase in a cell-free system. Biochem Biophys Res Commun. 1997; 230(1):206–10. https://doi.org/10.1006/bbrc.1996.5881 PMID: 9020047.

40. Chen J, He R, Minshall RD, Dinauer MC, Ye RD. Characterization of a mutation in the Phox homology domain of the NADPH oxidase component p40phox identifies a mechanism for negative regulation of superoxide production. J Biol Chem. 2007; 282(41):30273–84. https://doi.org/10.1074/jbc.M704416200 PMID: 17698849.

41. Dusi S, Della Bianca V, Donini M, Nadalini KA, Rossi F. Mechanisms of stimulation of the respiratory burst by TNF in nonadherent neutrophils: its independence of lipidic transmembrane signaling and dependence on protein tyrosine phosphorylation and cytoskeleton. J Immunol. 1996; 157(10):4615–23. PMID: 8906841.

42. Cheng G, Lambeth JD. NOXO1, regulation of lipid binding, localization, and activation of Nox1 by the Phox homology (PX) domain. J Biol Chem. 2004; 279(6):4737–42. https://doi.org/10.1074/jbc.M305968200 PMID: 14617635.

43. Miyano K, Ueno N, Takeya R, Sumimoto H. Direct involvement of the small GTPase Rac in activation of the superoxide-producing NADPH oxidase Nox1. J Biol Chem. 2006; 281(31):21857–68. https://doi.org/10.1074/jbc.M513665200 PMID: 16762923.

44. Heyworth PG, Bohl BP, Bokoch GM, Curnutte JT. Rac translocates independently of the neutrophil NADPH oxidase components p47phox and p67phox. Evidence for its interaction with flavocytochrome b558. J Biol Chem. 1994; 269(49):30749–52. PMID: 7982999.

45. Holzinger A. Jasplakinolide: an actin-specific reagent that promotes actin polymerization. Methods Mol Biol. 2009; 586:71–87. https://doi.org/10.1007/978-1-60761-376-3_4 PMID: 19768425.

46. Tam VC, Serruto D, Dziejman M, Brieher W, Mekalanos JJ. A type III secretion system in Vibrio cholerae translocates a formin/spire hybrid-like actin nucleator to promote intestinal colonization. Cell Host Microbe. 2007; 1(2):95–107. https://doi.org/10.1016/j.chom.2007.03.005 PMID: 18005688.

47. Tam VC, Suzuki M, Coughlin M, Saslowsky D, Biswas K, Lencer WI, et al. Functional analysis of VopF activity required for colonization in Vibrio cholerae. MBio. 2010; 1(5). https://doi.org/10.1128/mBio.00289-10 PMID: 21151774; PubMed Central PMCID: PMCPMC2999938.

48. Pernier J, Orban J, Avvaru BS, Jegou A, Romet-Lemonne G, Guichard B, et al. Dimeric WH2 domains in Vibrio VopF promote actin filament barbed-end uncapping and assisted elongation. Nat Struct Mol Biol. 2013; 20(9):1069–76. https://doi.org/10.1038/nsmb.2639 PMID: 23912276.

49. Hiyoshi H, Kodama T, Saito K, Gotoh K, Matsuda S, Akeda Y, et al. VopV, an F-actin-binding type III secretion effector, is required for Vibrio parahaemolyticus-induced enterotoxicity. Cell Host Microbe. 2011; 10(4):401–9. https://doi.org/10.1016/j.chom.2011.08.014 PMID: 22018240.

50. Zhou X, Gewurz BE, Ritchie JM, Takasaki K, Greenfeld H, Kieff E, et al. A Vibrio parahaemolyticus T3SS effector mediates pathogenesis by independently enabling intestinal colonization and inhibiting TAK1 activation. Cell Rep. 2013; 3(5):1690–702. https://doi.org/10.1016/j.celrep.2013.03.039 PMID: 23623501; PubMed Central PMCID: PMCPMC3711673.

51. Bylund J, Burgess LA, Cescutti P, Ernst RK, Speert DP. Exopolysaccharides from Burkholderia cenocepacia inhibit neutrophil chemotaxis and scavenge reactive oxygen species. J Biol Chem. 2006; 281 (5):2526–32. https://doi.org/10.1074/jbc.M510692200 PMID: 16316987.

52. Pedersen SS, Kharazmi A, Espersen F, Hoiby N. Pseudomonas aeruginosa alginate in cystic fibrosis sputum and the inflammatory response. Infect Immun. 1990; 58(10):3363–8. PMID: 2401567; PubMed Central PMCID: PMCPMC313661.

53. Lodge R, Diallo TO, Descoteaux A. Leishmania donovani lipophosphoglycan blocks NADPH oxidase assembly at the phagosome membrane. Cell Microbiol. 2006; 8(12):1922–31. https://doi.org/10.1111/j.1462-5822.2006.00758.x PMID: 16848789.

54. Siemsen DW, Kirpotina LN, Jutila MA, Quinn MT. Inhibition of the human neutrophil NADPH oxidase by Coxiella burnetii. Microbes Infect. 2009; 11(6–7):671–9. https://doi.org/10.1016/j.micinf.2009.04.005 PMID: 19379824; PubMed Central PMCID: PMCPMC2704257.

55. Harada T, Miyake M, Imai Y. Evasion of Legionella pneumophila from the bactericidal system by reactive oxygen species (ROS) in macrophages. Microbiol Immunol. 2007; 51(12):1161–70. PMID: 18094534.

56. McCaffrey RL, Allen LA. Francisella tularensis LVS evades killing by human neutrophils via inhibition of the respiratory burst and phagosome escape. J Leukoc Biol. 2006; 80(6):1224–30. https://doi.org/10.1189/jlb.0406287 PMID: 16908516; PubMed Central PMCID: PMCPMC1828114.

57. Vazquez-Torres A, Xu Y, Jones-Carson J, Holden DW, Lucia SM, Dinauer MC, et al. Salmonella pathogenicity island 2-dependent evasion of the phagocyte NADPH oxidase. Science. 2000; 287 (5458):1655–8. PMID: 10698741.

58. Henry T, Garcia-Del Portillo F, Gorvel JP. Identification of Salmonella functions critical for bacterial cell division within eukaryotic cells. Mol Microbiol. 2005; 56(1):252–67. https://doi.org/10.1111/j.1365-2958.2005.04540.x PMID: 15773994.

59. Rosenberger CM, Finlay BB. Macrophages inhibit Salmonella typhimurium replication through MEK/ERK kinase and phagocyte NADPH oxidase activities. J Biol Chem. 2002; 277(21):18753–62. https://doi.org/10.1074/jbc.M110649200 PMID: 11821396.

60. Vogel V, Sheetz MP. Cell fate regulation by coupling mechanical cycles to biochemical signaling pathways. Curr Opin Cell Biol. 2009; 21(1):38–46. https://doi.org/10.1016/j.ceb.2009.01.002 PMID: 19217273; PubMed Central PMCID: PMCPMC3792581.

61. Muller P, Langenbach A, Kaminski A, Rychly J. Modulating the actin cytoskeleton affects mechanically induced signal transduction and differentiation in mesenchymal stem cells. PLoS One. 2013; 8(7): e71283. https://doi.org/10.1371/journal.pone.0071283 PMID: 23923061; PubMed Central PMCID: PMCPMC3726577.

62. Trosky JE, Mukherjee S, Burdette DL, Roberts M, McCarter L, Siegel RM, et al. Inhibition of MAPK signaling pathways by VopA from Vibrio parahaemolyticus. J Biol Chem. 2004; 279(50):51953–7. https://doi.org/10.1074/jbc.M407001200 PMID: 15459200.

63. Trosky JE, Li Y, Mukherjee S, Keitany G, Ball H, Orth K. VopA inhibits ATP binding by acetylating the catalytic loop of MAPK kinases. J Biol Chem. 2007; 282(47):34299–305. https://doi.org/10.1074/jbc.M706970200 PMID: 17881352.

64. Mukherjee S, Keitany G, Li Y, Wang Y, Ball HL, Goldsmith EJ, et al. Yersinia YopJ acetylates and inhibits kinase activation by blocking phosphorylation. Science. 2006; 312(5777):1211–4. https://doi.org/10.1126/science.1126867 PMID: 16728640.

65. Dziejman M, Serruto D, Tam VC, Sturtevant D, Diraphat P, Faruque SM, et al. Genomic characterization of non-O1, non-O139 Vibrio cholerae reveals genes for a type III secretion system. Proc Natl Acad Sci U S A. 2005; 102(9):3465–70. https://doi.org/10.1073/pnas.0409918102 PMID: 15728357; PubMed Central PMCID: PMCPMC552950.

66. Park KS, Ono T, Rokuda M, Jang MH, Okada K, Iida T, et al. Functional characterization of two type III secretion systems of Vibrio parahaemolyticus. Infect Immun. 2004; 72(11):6659–65. https://doi.org/10.1128/IAI.72.11.6659-6665.2004 PMID: 15501799; PubMed Central PMCID: PMCPMC523034.

67. Subauste MC, Von Herrath M, Benard V, Chamberlain CE, Chuang TH, Chu K, et al. Rho family proteins modulate rapid apoptosis induced by cytotoxic T lymphocytes and Fas. J Biol Chem. 2000; 275 (13):9725–33. PMID: 10734125.